JCTC Journal of Chemical Theory and Computation

Article

pubs.acs.org/JCTC

Laplacian-Level Kinetic Energy Approximations Based on the Fourth-Order Gradient Expansion: Global Assessment and Application to the Subsystem Formulation of Density Functional Theory

Savio Laricchia,[†] Lucian A. Constantin,*[,†] Eduardo Fabiano,[‡] and Fabio Della Sala[‡,†]

[†]Center for Biomolecular Nanotechnologies @UNILE, Istituto Italiano di Tecnologia (IIT), Via Barsanti, 73010 Arnesano, Lecce, Italy

[‡]National Nanotechnology Laboratory (NNL), Istituto Nanoscienze-CNR, Via per Arnesano 16, 73100 Lecce, Italy

Supporting Information

ABSTRACT: We tested Laplacian-level meta-generalized gradient approximation (meta-GGA) noninteracting kinetic energy functionals based on the fourth-order gradient expansion (GE4). We considered several well-known Laplacian-level meta-GGAs from the literature (bare GE4, modified GE4, and the MGGA functional of Perdew and Constantin (*Phys. Rev. B* **2007**,75, 155109)), as well as two newly designed Laplacian-level kinetic energy functionals (L0.4 and L0.6). First, a general assessment of the different functionals is performed to test them for model systems (one-electron densities, Hooke's atom, and different jellium systems) and atomic and molecular kinetic energies as well as for their behavior with respect to density-scaling transformations. Finally, we assessed, for the first time, the performance of the different functionals for subsystem density functional theory (DFT) calculations on noncovalently interacting systems. We found that the different Laplacian-level meta-GGA kinetic functionals may improve the description of different properties of electronic systems, but no clear overall advantage is found over the best GGA functionals. Concerning the subsystem DFT calculations, the here-proposed L0.4 and L0.6 kinetic energy functionals are competitive with state-of-the-art GGAs, whereas all other Laplacian-level functionals fail badly. The performance of the Laplacian-level functionals is rationalized thanks to a two-dimensional reduced-gradient and reduced-Laplacian decomposition of the nonadditive kinetic energy density.

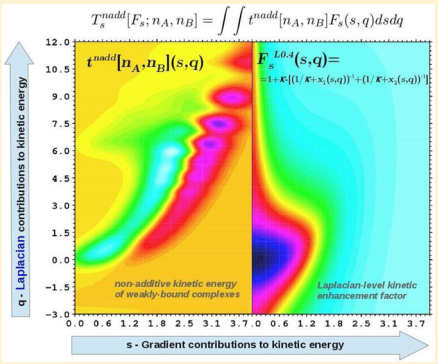

1. INTRODUCTION

The noninteracting kinetic energy (KE) density functional has been the subject of intense research in electronic structure theory for almost one century, since the introduction of the Thomas−Fermi model.[1−3] This interest has been further motivated, and theoretically justified, by the introduction of the density functional theory (DFT),[4,5] which has the noninteracting KE as a main ingredient. In the orbital-free formulation of DFT,[4,6,7] the noninteracting KE density functional is, in fact, the main contribution to the electronic energy, which has no explicit analytical expression in terms of the density (the other term being the exchange-correlation (XC) functional). Despite the effort spent on it,[8−68] however, the development of accurate non-interacting KE functionals resulted to be an extremely difficult task. As a consequence, orbital-free DFT is still of limited practical utility, showing reasonable accuracy only for some solid-state applications.[39−41,69−76] Recently, the density-decomposed orbital-free DFT, that treats differently the localized and delocalized densities, seems to have brought further progress to the field.[77,78] We also acknowledge that the possibility of reaching chemical accuracy within orbital-free DFT calculations was proved recently, at least for one-dimensional systems, by calculations employing machine learning techniques to approximate the noninteracting kinetic energy (with $\sim 10^5$ parameters).[79] However, this study also showed the extreme difficulty of this problem.

On the other hand, in recent years, the interest in KE functionals was strongly renewed by the development of density embedding methods,[69,80−91] where a many electron system with electron density $n(\mathbf{r})$ is partitioned into two subsystems A and B, such that the total electron density is $n = n_A + n_B$, and the mutual interaction is accounted for by an appropriate embedding potential. Of special relevance in this context is the subsystem formulation of DFT within the Kohn−Sham formalism.[83,84] In the standard formulation of this method, the system is described by two coupled sets of Kohn−Sham equations with constrained electron density (KSCED[83]). Hence, the density is constrained to satisfy the condition $n = n_A + n_B$ by the inclusion of an external embedding potential of the form (here the embedding potential for subsystem A is reported; a similar expression holds for B)

$$v_{\mathrm{emb}}^{\mathrm{A}}[n_{\mathrm{A}};n_{\mathrm{B}}](\mathbf{r}) = v_{\mathrm{ext}}^{\mathrm{B}}(\mathbf{r}) + v_J[n_{\mathrm{B}}](\mathbf{r}) + \frac{\delta E_{\mathrm{xc}}^{\mathrm{nadd}}[n_{\mathrm{A}};n_{\mathrm{B}}]}{\delta n_{\mathrm{A}}(\mathbf{r})} + \frac{\delta T_{\mathrm{s}}^{\mathrm{nadd}}[n_{\mathrm{A}};n_{\mathrm{B}}]}{\delta n_{\mathrm{A}}(\mathbf{r})} \quad (1)$$

Received: September 23, 2013
Published: December 11, 2013

where $v_{ext}^{B}(\mathbf{r})$ and $v_J[n_B](\mathbf{r})$ are the external (i.e., nuclear) and the Coulomb potentials due to subsystem B, while the nonadditive XC and kinetic energy terms are defined as

$$E_{xc}^{nadd}[n_A;n_B] = E_{xc}[n_A + n_B] - E_{xc}[n_A] - E_{xc}[n_B] \quad (2)$$

$$T_s^{nadd}[n_A;n_B] = T_s[n_A + n_B] - T_s[n_A] - T_s[n_B] \quad (3)$$

Using an iterative freeze-and-thaw procedure[84,92] the full variational solution for the total system can be obtained, which is equivalent to the usual Kohn−Sham solution, except for approximations included in the nonadditive kinetic interaction term and eventually in the nonadditive XC contribution, if hybrid or orbital-dependent functionals are employed in the subsystem formalism.[89,90,93,94] Henceforth, the acronym FDE will be used to refer to this fully variational approach.

As shown by eqs 1 and 3, the accuracy of the FDE method relies on the availability of accurate kinetic energy approximations. However, unlike for orbital-free DFT, the FDE approach makes use not of the bare noninteracting KE, but rather of the nonadditive KE contribution (the remaining part of the kinetic energy, i.e., the subsystems' KE, is treated in a Kohn−Sham fashion within the KSCED equations[84,92]). For nonbonded interactions, the nonadditive KE is quite small and well-behaved, so that, in analogy to the XC energy, it can be efficiently described by semilocal approximations. Thus, for a broad range of problems (e.g., hydrogen bonds, dipole−dipole, and dispersion complexes), the FDE method can reach a high performance, often below the chemical accuracy.[62,64]

Motivated by the practical appeal of the FDE method, in the last years, different semilocal KE approximations were proposed to describe the nonadditive KE bifunctional.[36,37,61−64,95] However, all these approximations are making use only of the simplest semilocal ingredients, i.e., the density n and its gradient ∇n, being based on the generalized gradient approximation (GGA). Comparison with the experience accumulated for the much widely investigated XC functional shows nevertheless that the GGA level has some inevitable limitations due to its intrinsic simplicity and, in particular, cannot properly distinguish between different density regimes.[63,64]

Thus, the investigation of the performance of more sophisticated functionals beyond the GGA level (meta-GGA functionals) in the context of the FDE method is of high interest. To date, however, to our knowledge, no such study has ever been performed. For this reason, this work has as principal goal to perform a general assessment of some existing[23,55] and new Laplacian-level meta-GGA KE functionals in the context of the FDE method. This study will be performed by first testing the general quality of the KE functionals on a wide set of systems and properties. Then, direct application of the KE functionals in FDE calculations will be considered.

At this point, it is important, however, to note that most meta-GGA XC functionals are implemented using as additional ingredient to the GGA ones, the positive-defined kinetic energy density $\tau = (1/2)\Sigma_i^{occ}|\nabla\phi_i|^2$, where ϕ_i are the occupied Kohn−Sham orbitals. The Laplacian of the density instead is not used directly but mimicked in the atomic core through a function depending on n, ∇n, and τ.[96,97] This choice is convenient because the positive-defined kinetic energy density has a more regular behavior than $\nabla^2 n$, which oscillates and diverges near the atomic nucleus. At the same time, the use of τ causes the so constructed meta-GGA functionals to have a nonlocal dependence on the density (via the orbital-dependent τ).

The focus of this paper is on meta-GGA KE functionals using the Laplacian of the density as a meta-GGA ingredient. In this way, despite some possible limitations due to the behavior of $\nabla^2 n$, it is possible to construct a truly semilocal KE functional suitable to be used in the FDE formalism and having meta-GGA quality. We recall in fact that $\nabla^2 n$ is an important ingredient for the construction of functionals and enters in the definition of the fourth- and higher-order gradient expansions of the exact kinetic energy.[23]

2. KINETIC ENERGY FUNCTIONALS

A Laplacian-level semilocal KE functional has the general form

$$T_s[n] = \int d\mathbf{r};\ \tau^{TF} F_s(n, \nabla n, \nabla^2 n) \quad (4)$$

where $\tau^{TF} = (3/10)(3\pi^2)^{2/3} n^{5/3}$ is the Thomas−Fermi kinetic energy density,[1−3] and F_s is a suitable kinetic enhancement factor. Under a uniform scaling of the density ($n_\lambda(\mathbf{r}) = \lambda^3 n(\lambda\mathbf{r})$, $\lambda \geq 0$), the exact noninteracting kinetic energy behaves as $T_s[n_\lambda] = \lambda^2 T_s[n]$, i.e., as the Thomas−Fermi KE. Therefore, to have eq 4 satisfy this constraint, $F_s(n, \nabla n, \nabla^2 n,...)$ must be invariant under the uniform density scaling. Such a goal can be achieved by considering the following dimensionless reduced gradient and Laplacian

$$p = \frac{|\nabla n|^2}{4(3\pi^2)^{2/3} n^{8/3}}; \qquad q = \frac{\nabla^2 n}{4(3\pi^2)^{2/3} n^{5/3}} \quad (5)$$

The enhancement factor becomes therefore

$$F_s(n, \nabla n, \nabla^2 n) = F_s(p,q) \quad (6)$$

In this paper we consider the following approximations for the kinetic enhancement factor:

(i) **Thomas-Fermi** (TF), defined as

$$F_s^{TF} = 1 + aq \quad (7)$$

with a a parameter. This is the simplest approximation and becomes exact for the uniform electron gas, as well for any region of space where the density is constant. The term aq integrates to zero and is unimportant for the kinetic energy and its functional derivative. Thus, usually the parameter a is set to zero. However, it was shown that $a = 5/3$ improves the quality of the TF KE density[98] (not relevant for the present work).

(ii) Second-order gradient expansion (GE2),[15] defined as

$$F_s^{GE2} = 1 + \frac{5}{27}p + \frac{20}{9}q \quad (8)$$

As for the TF case, the last term in eq 8 integrates to zero and does not contribute to the kinetic energy and potential. Therefore, it is usually disregarded in most applications.

(iii) Fourth-order gradient expansion (GE4),[23] written as

$$F_s^{GE4} = F_s^{GE2} + \Delta \quad (9)$$

with

$$\Delta = \frac{8}{81}q^2 - \frac{1}{9}pq + \frac{8}{243}p^2 \geq 0 \quad (10)$$

This enhancement factor is a simplified version, obtained via the Green's theorem integration of terms comprising higher-order derivatives of the density. It holds for finite systems under the assumption that $n(\mathbf{r})$ and $\nabla n(\mathbf{r})$ vanish as $r \to \infty$. For the full GE4 expression, see refs 5 and 15. We note that the GE4 KE displays a serious drawback for finite systems, as it shows

dx.doi.org/10.1021/ct400836s | J. Chem. Theory Comput. 2014, 10, 164−179

the wrong behavior in the tail of the density of a finite system. In this region, in fact, the density decays exponentially as $n \sim e^{-\alpha r}$, and the von Weizsäcker KE is almost exact. Hence, the exact kinetic energy density behaves as $\tau \sim \tau^{W} \sim \tau^{GE2} \sim n$. On the other hand, we have $\tau^{GE4} \sim n^{1/3}$ being much worse than GE2. Moreover, the corresponding potential diverges under the same conditions. This behavior is not surprising if we consider that higher-order gradient expansion terms are derived from small perturbations of the uniform electron gas, so that they contain the right physics for a slowly varying density regime but fail in rapidly varying regions, such as in the tail of finite systems or near the nucleus. For this reason, GE4 usually worsens the atomic KE with respect to GE2. Similarly, the sixth-order gradient expansion (GE6)[12] that contains terms of order $O(p^3,q^3,q^2p,...)$ has a kinetic energy density that even diverges in the tail of the density of a finite system ($\tau^{GE6} \sim n^{-1/3}$). Consequently, the GE6 KE diverges for any finite system.

(iv) Modified fourth-order gradient expansion (MGE4), defined by

$$F_s^{MGE4} = F_s^{GE4} \Big/ \sqrt{1 + \left(\frac{\Delta}{1 + \frac{5}{3}p}\right)^2} \tag{11}$$

This construction was proposed in ref 55 and recovers GE4 for a slowly varying density. Instead, near the nucleus and in the tail of an atom (when $|q| \to \infty$) $F_s^{MGE4} \to 1 + F_s^{W}$, with $F_s^{W} = 5/3p$, the von Weizsäcker (W) enhancement factor.[8] This latter is a much reasonable limit for rapidly varying density regions and is also the correct limit for a uniform density perturbed by a small-amplitude short-wavelength density wave.[22]

(v) The **Laplacian-level meta-GGA** (MGGA),[55] with the following expression

$$F_s^{MGGA} = F_s^{W} + (F_s^{MGE4} - F_s^{W}) f_{ab}(F_s^{MGE4} - F_s^{W}) \tag{12}$$

where

$$f_{ab}(z) = \begin{cases} 0 & z \le 0 \\ \left(\dfrac{1 + e^{a/(a-z)}}{e^{a/z} + e^{a/(a-z)}}\right) & 0 < z < a \\ 1 & z \ge a \end{cases} \tag{13}$$

is an analytical real-valued sharp-interpolating function, with $a = 0.5389$ and $b = 3$. Note that $F_s^{MGE4}-F_s^{W}$ is adimensional.[55] MGGA is one of the best models for the exact kinetic energy density, fulfilling many exact conditions, as the rigorous lower bound[55,99]

$$\tau^{W}(\mathbf{r}) \le \tau(\mathbf{r}) \tag{14}$$

(vi) In addition to the models listed above, in this work, we consider also a new Laplacian-level meta-GGA KE approximation defined by the simple ansatz

$$F_s^{L\kappa} = 1 + 2\kappa - \left(\frac{\kappa}{1 + \frac{x_1}{\kappa}} + \frac{\kappa}{1 + \frac{x_2}{\kappa}}\right) \tag{15}$$

with

$$x_1 = \frac{5}{27}p + \Delta + \frac{\left(\frac{5}{27}p\right)^2}{\kappa} \tag{16}$$

$$x_2 = 2\frac{\left(\frac{5}{27}p\right)\Delta}{\kappa} + \frac{\left(\frac{5}{27}p\right)^3}{\kappa^2} \tag{17}$$

This functional is designed to respect the following limits:

(1) In the slowly varying density limit (s and $q \to 0$), it behaves as

$$F_s^{L\kappa} \to 1 + \frac{5}{27}p + \Delta + O(p^4, q^4, p^3q, ...) \tag{18}$$

therefore, it recovers GE4, except for the unimportant term $(20/9)q$. Note also that eq 18 does not contain terms of a sixth order (e.g., $(|\nabla n|)^6$), so that it recovers GE4 quite closely for a wider range of (small) values of s and q.

(2) In the rapidly varying density limit (s or $|q| \to \infty$), it behaves as

$$F_s^{L\kappa} \to 1 + 2\kappa \tag{19}$$

Thus, it can be made to recover the behavior of the APBEK[63,64] or revAPBEK[63,64] functionals in the rapidly varying density limit. Consequently, we define two variants of the functional

L0.4 where $\kappa = \frac{1}{2}\kappa^{APBEK} = 0.402$

L0.6 where $\kappa = \frac{1}{2}\kappa^{revAPBEK} = 0.623$

We constructed the L0.4/L0.6 functionals in order to recover the APBEK/revAPBEK limit because the latter functionals have been found to yield very accurate embedding energies still keeping good accuracy for other properties (total and relative kinetic energies).[63,64] On the other hand, recent works at the GGA level[62,64] found that functionals diverging at large s are very poor for the embedding theory.

We remark that the MGE4, MGGA, L0.4, and L0.6 functionals recover the GE4 limit, whereas other Laplacian-level meta-GGA KE functionals, e.g., those in refs 67, 68, and 100 do not. Thus, the latter functionals are not considered in this work.

Figure 1 shows several enhancement factors as functions of the reduced gradient $s = p^{1/2}$. The plots are reported for two values of q in the range appropriate to physical densities ($q = 0$ and $q = 2$). For GE2, W (von Weizsäcker), GE4, MGE4, and MGGA, we subtracted in the plot the term $(20/9)q$ to have a more direct comparison with L0.4 and L0.6 that do not include such a term. Two-dimensional plots in the (s,q)-space for all Laplacian-based KE functionals listed in this section are reported in the Supporting Information.

For $q = 0$ (upper panel), all functionals behave similarly in the small s region ($s \lesssim 0.7$), recovering the modified GE2 (in the case of APBEK and revAPBEK GGAs) or the GE4 (in case of Laplacian-based functionals) (see the inset in the upper panel of Figure 1). At medium values of s ($0.7 \lesssim s \lesssim 1.7$), MGE4, L0.4, and L0.6 still recover, by construction, the GE4 behavior. On the other hand, MGGA shows an unphysical strong oscillation due to the sharp interpolation function (eq 13). Finally, at large values of s, GE4, MGE4, and MGGA diverge, whereas the L0.4 and L0.6 functionals show a saturation toward the APBEK and revAPBEK limits. Note, however, that these limits are only reached at very large values of the reduced gradient. Moreover, all the functionals but MGGA fail to respect the exact constraint $F_s \ge F_s^{W}$.

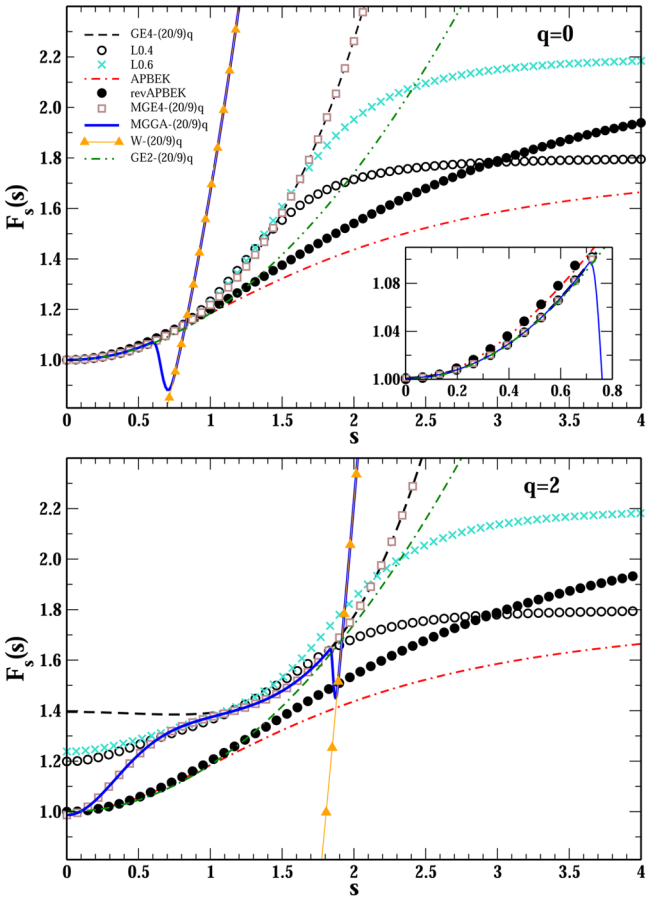

Figure 1. KE enhancement factors for several functionals as functions of the reduced gradient s ($s = p^{1/2}$) in the case of $q = 0$ (upper panel) and $q = 2$ (lower panel). For GE2, W, GE4, MGE4, and MGGA, we subtracted in the plot the term $(20/9)q$.

For $q = 2$ (lower panel), a moderately varying density regime is considered. The picture does not change much for large s values, but it is drastically modified for small values of the reduced gradient. Note, however, that for the GGA functionals (APBEK and revAPBEK) we have of course the same plot as for the previous case. In this case, at medium values of s, all Laplacian-level meta-GGA functionals agree rather well, except for the unphysical oscillations displayed by MGGA. For small s values ($s \to 0$), different behaviors are observed. MGE4 and MGGA have the same trend and move toward Thomas−Fermi; GE4 tends to $1 + (8/81)q^2 \approx 1.395$ displaying its well-known divergent behavior in this regime; and finally, the L0.4 and L0.6 functionals tend to

$$F_s^{L\kappa} \to 1 + 2\kappa - \left(\frac{\kappa}{1 + \frac{8}{81}\frac{q^2}{\kappa}} + \kappa \right) \tag{20}$$

that is $F_s^{L0.4} \to 1.20$ and $F_s^{L0.6} \to 1.24$.

The density regime characterized by $s = 0$ and q finite is important in the middle of molecular bonds. In order to understand better this density regime, we report in Figure 2 $\partial^2 F_s(s = 0,q)/\partial q^2$ versus q for several enhancement factors. Note that $\partial^2 F_s(s,q)/\partial q^2$ is an intrinsic quantity of the enhancement factor, being independent of the linear $(20/9)q$ term. As reference, we consider the exact Kohn−Sham KE enhancement factor derivative $(\partial^2 F_s^{exact}(s = 0,q)/\partial q^2)$ (computed numerically) in the middle of the bond between two interacting jellium slabs of $r_s = 3$ and a thickness of $2\lambda_F$ each (with $\lambda_F = 2\pi/k_F$ being the Fermi wavelength). When the jellium slabs are close to each other ($z \ll \lambda_F$), q is small (and positive) at the bond, and when the jellium slabs are far from each other ($z \geq \lambda_F$), q is large (and positive). While MGE4 and MGGA show strong oscillations, the Lκ functionals perform remarkably smooth and close to the reference. Note that in case $s = 0$ and $q \to 0$, the reference curve contains higher-order terms that are out of reach for GE4-based functionals.

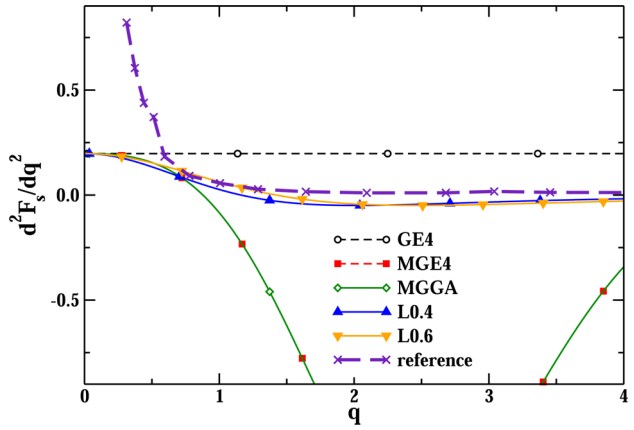

Figure 2. $\partial^2 F_s(p = 0,q)/\partial q^2$ versus q for several enhancement factors.

3. DENSITY-SCALING BEHAVIOR

Consider the family of density scalings[101]

$$n_\lambda(\mathbf{r}) = \lambda^{3\beta+1} n(\lambda^\beta \mathbf{r}), \quad \lambda > 0 \tag{21}$$

where β is a parameter, which is changing not only the external potential associated with the density n (as in the uniform density scaling) but also the particle number ($N \to \lambda N$). Under this scaling, the KE gradient expansion terms behave as[101]

$$T_s^{TF}[n_\lambda] = \lambda^{2\beta+5/3} T_s^{TF}[n] \tag{22a}$$

$$T_s^{(2)}[n_\lambda] = \frac{1}{9} T_s^{W}[n_\lambda] = \frac{1}{9} \lambda^{2\beta+1} T_s^{W}[n] \tag{22b}$$

$$T_s^{(4)}[n_\lambda] = \lambda^{2\beta+1/3} T_s^{(4)}[n] \tag{22c}$$

where $T_s^{(2)} = \int d\mathbf{r}\, \tau^{TF}[(5/27)p + (20/9)q]$ and $T_s^{(4)} = \int d\mathbf{r}\, \tau^{TF} \Delta(p,q)$ are the second- and fourth-order terms of the KE gradient expansion, respectively. On the other hand, the reduced gradient s and the reduced Laplacian q scale as $s_\lambda(\mathbf{r}) = \lambda^{-1/3} s(\lambda^\beta \mathbf{r})$ and $q_\lambda(\mathbf{r}) = \lambda^{-2/3} q(\lambda^\beta \mathbf{r})$, respectively. Thus, the reduced gradient and Laplacian are independent of β, and the slowly varying density limit ($s,q \to 0$) is reached whenever $\lambda \to \infty$. For $\lambda \ll 1$, instead, a rapidly varying density regime is always set up.

For different values of the parameter β, eq 21 spans an impressive number of physical properties. Some of them are analyzed in the next subsections.

3.1. Thomas−Fermi Scaling. For $\beta = 1/3$, the Thomas−Fermi scaling is obtained. In the limit $\lambda \to \infty$, any system resembles the features of the Thomas−Fermi density.[102] The Thomas−Fermi scaling is the basis for the asymptotic expansion of the kinetic energy[100,103,104]

$$T_s = c_0 \lambda^{7/3} + c_1 \lambda^2 + c_2 \lambda^{5/3} + \ldots \tag{23}$$

dx.doi.org/10.1021/ct400836s | J. Chem. Theory Comput. 2014, 10, 164−179

Table 1. Error Statistics for Different Density Scaling Tests[a]

	GGAs				meta-GGAs				
	TF	GE2	APBEK	revAPBEK	GE4	MGE4	MGGA	L0.4	L0.6
Thomas-Fermi scaling (β = 1/3)									
Δc_1	−160.87	−36.25	−3.77	−2.20	−20.39	−17.28	**−8.90**	<u>−23.40</u>	−22.39
Δc_2	115.50	66.13	17.14	27.00	73.25	72.84	**47.53**	<u>79.04</u>	74.75
Homogeneous scaling (β = 0)									
Δs_{eff}	0.67	0.55	0.59	0.58	0.47	0.49	**0.02**	<u>0.54</u>	0.53
Fractional scaling (β = 1)									
Δs_{eff}	0.67	0.47	0.50	0.50	0.38	0.42	**0.02**	<u>0.45</u>	0.44
ΔM	12.26	34.71	33.84	35.89	38.05	<u>38.89</u>	**7.77**	37.15	37.15

[a]The best Laplacian-level meta-GGA result in each line is highlighted in bold face; the worst Laplacian-level meta-GGA result for each test is underlined.

with the coefficients, $c_0 = 0.768745$, $c_1 = -0.5$, and $c_2 = 0.2699$, fixed from the semiclassical theory of the neutral atom. The expansion of eq 23 is very accurate even for real atoms with errors on the order of 0.5−0.2%.

Using the method proposed in ref 100, we extracted the coefficients c_1 and c_2 for all the functionals considered in this work. We assumed that, because all the functionals recover TF for a constant density, they have the exact c_0 coefficient.

The deviations

$$\Delta c_i = 1000(c_i^{approx} - c_i^{exact}) \qquad i = 1,2 \tag{24}$$

are reported in Table 1 for each functional. As it might be expected, the best results are found for revAPBEK and APBEK, which were constructed from the semiclassical theory of the neutral atom. The Laplacian-level meta-GGAs provide a good performance, improving over GE2 for c_1, which is the leading term of quantum effects, beyond the Thomas−Fermi theory.

3.2. Uniform Electron Gas Scaling. The uniform electron gas scaling is obtained for $\beta = -(1/3)$ and $\lambda \to \infty$. Under these conditions, in fact, the density varies very slowly, being almost constant over the space. Hence, the gradient expansion

$$T_s^{exact}[n_\lambda] = T_s^{TF}[n_\lambda] + T_s^{(2)}[n_\lambda] + T_s^{(4)}[n_\lambda] + T_s^{(6)}[n_\lambda] + ... \tag{25}$$

that was derived from small perturbations of the uniform electron gas is (almost) exact in this limit. As a consequence, all the Laplacian-level meta-GGA kinetic functionals, which recover GE4 in the slowly varying density, become very accurate under the uniform electron gas scaling.

3.3. Homogeneous Scaling. Setting $\beta = 0$ and considering the limit $\lambda \to 0$, the homogeneous scaling is realized.[101,105−109] This scaling is a valuable tool in DFT and was used to study the static correlation[110,111] and the delocalization error,[111] as well as to construct kinetic energy functionals.[112]

Following ref 101, we study the ability of different functionals to satisfy the homogeneous scaling by considering the hydrogen density n_H and the associated effective scaling order

$$s_{eff} = \int_0^1 \frac{\ln(|T_s[n_H]|) - \ln(|T_s[n_{H\lambda}]|)}{\ln(\lambda)} d\lambda \tag{26}$$

This provides a measure for the scaling behavior of a generic KE functional. The exact result is $s_{eff}^{exact} = 1$ (W is the exact functional for the hydrogen atom; see eq 22b).

The errors on s_{eff} for different functionals are reported in Table 1. All the Laplacian-level meta-GGA functionals perform slightly better than GGA ones, showing that the inclusion of the Laplacian dependence can help to improve the physical behavior of the functional. Notably, the MGGA functional stands out over the other meta-GGAs, scaling almost perfectly under the homogeneous scaling. This finding supports the conclusion that this sophisticated approximation can capture very well the physics of the von Weizsäcker functional.

3.4. Fractional Scaling. The fractional scaling is defined by $\beta = 1$ and the limit $\lambda \to 0$. It describes the physics of systems with a fractional number of electrons.[101] In particular, the fractional scaling is related to the disintegration of the hydrogen atom into fragments with fractional nuclear and electronic charge, which is a model for atomization processes in molecules.[101]

In analogy with ref 101, we define the kinetic disintegration energy of the hydrogen atom into fragments with partial charge λ and $1 - \lambda$ as

$$M(\lambda) = T_s(1) - T_s(\lambda) - T_s(1 - \lambda) \tag{27}$$

where $T_s(1)$ is the kinetic energy of the hydrogen atom, and $T_s(\lambda)$ is the KE of the neutral fragment with charge λ. The disintegration error is then defined as

$$\Delta M = \int_0^1 [M^{DFT}(\lambda) - M^{exact}(\lambda)] d\lambda \tag{28}$$

In Table 1, we report for all the functionals the errors on the effective scaling order (eq 26), with respect to the exact result $s_{eff} = 3$ and the disintegration error of eq 28. The results show that the effective scaling order follows a similar trend as for the homogeneous scaling. The inspection of the values of ΔM provides a couple of additional considerations that shows the importance of fractional scaling: (1) The MGGA functional works very well for both s_{eff} and the disintegration problem, showing that this functional can incorporate most of the von Weizsäcker[8] physics without error compensations. (2) The TF functional displays the worst s_{eff} value but the smallest error for the disintegration problem (except for MGGA), showing an important error cancellation.

4. COMPUTATIONAL DETAILS

4.1. Kinetic Energies. To test the different functionals, we assessed their ability to compute the KE of different systems:

Model One- and Two-electron Systems. These include the one-electron Gaussian, hydrogen, and cuspless-hydrogen densities, as well as the Hooke's atom at various values of the harmonic potential. For these systems, the reference values were computed via the von Weizsäcker formula. In all calculations, exact densities were employed.

Jellium Systems. We considered (i) a series of Na jellium clusters ($r_s = 3.93$) with magic electron numbers of 2, 8, 18, 20,

Table 2. Mean Absolute Relative Errors (MARE) in % for Different Tests and Absolute Relative Errors for One-Electron Densities (G, H, and C)[a]

	GGAs				meta-GGAs				
	TF	GE2	APBEK	revAPBEK	GE4	MGE4	MGGA	L0.4	L0.6
Total kinetic energies									
H	8.2	2.9	2.2	3.1	5.8	5.5	**2.5**	4.4	4.5
G	10.1	1.0	1.8	0.8	15.3	4.2	3.7	∗**0.7**	1.3
C	5.3	5.8	4.6	5.6	8.9	7.9	∗**2.1**	6.8	9.6
Hooke's atom KE	25.7	14.6	18.8	17.8	14.6	∗**10.3**	∗14.3	15.5	∗14.5
Jell. clust. KE	4.4	1.0	1.0	0.8	1.9	1.2	2.5	**0.9**	1.0
Jell. slabs KE	1.89	0.57	0.55	0.46	∗**0.21**	∗0.36	∗0.36	∗0.42	∗0.39
Atoms' KE	8.4	1.1	0.8	1.2	2.5	2.4	**1.4**	1.9	2.0
Molecules' KE	9.7	0.9	0.5	0.4	1.0	1.2	1.4	**0.8**	**0.8**
MARE(GE2)	5.42	1	0.94	0.88	2.16	1.42	1.43	**1.07**	1.15
Kinetic energy differences									
Jell. clust. DKE	17.7	27.2	18.9	23.1	50.2	39.0	∗**17.9**	29.3	31.5
Jell. surf. LDM	8.1	3.3	3.9	3.6	∗**1.7**	∗1.9	∗2.5	∗2.8	∗2.8
Jell. slabs DKE	17.28	5.02	4.17	3.45	∗**1.31**	3.53	3.53	∗2.85	∗2.65
Atoms' IKE	49.5	42.2	45.8	44.4	∗**39.2**	∗40.7	51.8	∗41.3	∗41.4
Molecules' AKE	106.0	184.0	142.0	155.0	222.0	207.0	∗**108.0**	216.0	217.0
MARE(GE2)	1.66	1.00	0.91	0.90	0.95	0.96	∗**0.79**	0.93	0.94

[a]The best Laplacian-level meta-GGA result in each line is highlighted in bold face; the worst Laplacian-level meta-GGA result for each test is underlined. The last line reports the MARE relative to the GE2 performance (see text for details). The star symbol stands for a Laplacian-level meta-GGA KE functional that is better than the best GGA.

34, 40, 58, 92, and 106, used also in refs 55, 56, and 64, (**ii**) jellium surfaces with bulk parameter r_s = 2, 4, and 6 into the liquid drop model (LDM) (as in refs 55, 56, and 64), and (**iii**) two interacting jellium slabs at different distances. Each jellium slab has r_s = 3 and a thickness of $2\lambda_F$.

All the calculations were performed using the orbitals and densities resulting from numerical Kohn–Sham calculations within the local density approximation[113] for the exchange-correlation functional ((**ii**) and (**iii**)) and the exact exchange functional ((**i**)).

Atoms and Ions. We tested the benchmark set of atoms and ions used in refs 55, 56, and 64. All calculations employed analytic Hartree–Fock orbitals and densities.[114] We also calculated the ionization KE of noble atoms (until Uuo) using accurate exact-exchange Kohn–Sham densities and orbitals.

Molecules. We considered the set of molecules including H_2, HF, H_2O, CH_4, NH_3, CO, F_2, HCN, N_2, CN, NO, and O_2. This set was already used in refs 55, 56, and 115. The noninteracting kinetic energies of test molecules were calculated using the PROAIMV code.[116] The required Kohn–Sham orbitals were obtained by Kohn–Sham calculations performed with the uncontracted 6-311+G(3df,2p) basis set, the Becke 1988 exchange functional,[117] and Perdew–Wang correlation functional.[118]

4.2. FDE Calculations. The FDE calculations were performed using the FDE script as implemented in the TURBOMOLE program package.[119] Details about our KSCED implementation in TURBOMOLE are discussed in refs 64 and 89. The implementation of Laplacian-level meta-GGA functionals is briefly discussed in the Appendix. In all calculations, the PBE[120] XC functional and def2-TZVPPD monomolecular basis set[121,122] were used. The use of a monomolecular approach was needed to guarantee good convergence for calculations using the MGE4 and MGGA KE functionals. These functionals show in fact marked oscillations in the KE potential in the tail of the density. Therefore, they can give rise to important numerical problems in a supermolecular basis set calculation. Results for the supermolecular basis set calculations are reported in the Supporting Information. The quality of our results was tested by comparing monomolecular and supermolecular results for the GGA KE functionals as well checking the convergence with increasingly large basis sets. We found that the def2-TZVPPD basis set, adding diffuse basis functions to the def2-TZVPP[121] basis, provides finally a reliable description of all the systems considered in this paper.

The FDE calculations were performed on the following test systems, characterized by different interaction characters: He–Ne, He–Ar, Ne–Ne, Ne–Ar, CH_4–Ne, C_6H_6–Ne, and CH_4–CH_4 (weak interaction); H_2S–H_2S, HCl–HCl, H_2S–HCl, CH_3Cl–HCl, CH_3SH–HCN, and CH_3SH–HCl (dipole–dipole interaction); and NH_3–NH_3, HCl–HCl, H_2O–H_2O, NH_3–H_2O, HF–NCH, $(HCONH_2)_2$, and $(HCOOH)_2$ (hydrogen bond). The geometry of the complexes was taken from refs 85, 123, and 124. The subsystems A and B are the monomer units.

The error on the total embedding energy was computed as[89,93]

$$\Delta E = E^{FDE}[n_A;n_B] - E^{KS}[n^{KS}] \tag{29}$$

where $E^{FDE}[n_A;n_B]$ is the FDE total energy obtained from the embedded subsystem densities n_A and n_B, whereas E^{KS} is the conventional Kohn–Sham total energy corresponding to the ground state density n^{KS}. The performance of the different approaches was evaluated within each group of molecules by computing the mean absolute error (MAE).

The errors on the embedding densities were studied by considering the deformation density

$$\Delta n(\mathbf{r}) = n_A(\mathbf{r}) + n_B(\mathbf{r}) - n^{KS}(\mathbf{r}) \tag{30}$$

Some plots for different systems were realized by representing the plane-averaged deformation density

$$\langle \Delta n \rangle_{xy}(z) = \int\int |\Delta n(x, y, z)| dx dy \tag{31}$$

dx.doi.org/10.1021/ct400836s | J. Chem. Theory Comput. 2014, 10, 164–179

where we used Cartesian coordinates explicitly, and the z direction is along the intermolecular axis. Finally, a quantitative measurement of the absolute error associated with a given embedding density was obtained by computing the embedding density error

$$\xi = \frac{1000}{N} \int |\Delta n(\mathbf{r})| d\mathbf{r} \tag{32}$$

with N the number of electrons. In the evaluation of ξ, only valence electron densities were considered. Core densities are in fact much higher than valence ones and would largely dominate the calculation of ξ. On the other hand, core densities are not very important for the determination of chemical and physical properties of the interaction between the subsystems, which are of interest here.

5. KINETIC ENERGIES OF MODEL SYSTEMS

In this section, we present the KE results of one-electron densities, the Hooke's atom, jellium surfaces, jellium clusters, interacting jellium slabs, atomic systems, and molecules. All results are summarized in Table 2, where we report mean absolute relative errors (MARE) for each test. In addition, the last line shows the average performance relative to the GE2 method, defined as

$$\mathrm{MARE(GE2)} = \frac{1}{N} \sum_{i=1}^{N} \frac{\mathrm{MARE}_i}{\mathrm{MARE}_{\mathrm{GE2}}} \tag{33}$$

where the sum runs over all the N tests, and MARE_i is the MARE of the i-th test.

5.1. One-Electron Densities. We tested the different KE functionals on three model one-electron densities, namely, the hydrogen (H), Gaussian (G), and cuspless (C) densities. These are defined as

$$n_{\mathrm{H}}(r) = \frac{e^{-2r}}{\pi}, \; n_{\mathrm{G}}(r) = \frac{e^{-r^2}}{\pi^{3/2}}, \; n_{\mathrm{C}}(r) = \frac{(1+r)e^{-r}}{32\pi} \tag{34}$$

They were used in the construction of several XC functionals,[97,125,126] being simple models for simple iso-orbital regions.

For these model densities, the von Weizsäcker[8] functional is exact and behaves as $\tau^{\mathrm{W}} \sim n$. A similar behavior is found for GE2 and all the GGAs, which therefore perform rather well for this problem, with errors below 6%. On the other hand, for GE4, in iso-orbital regions, we have $\tau^{\mathrm{GE4}} \sim n^{1/3}$. For this reason, GE4 performs significantly worse than GE2 in all cases (errors up to 15%) (note that it is in general also worse than TF, that has $\tau^{\mathrm{TF}} \sim n^{5/3}$). Finally, the correct behavior is restored for the other Laplacian-level meta-GGAs, which thus describe these one-electron densities reasonably well. In particular, in two cases, Laplacian-level meta-GGA functionals are more accurate than the best GGA functional. MGGA is the most accurate for the delocalized C density, and the L0.4 functional is the most accurate for the Gaussian density.

5.2. Hooke's Atom. Hooke's atom consists of two interacting electrons in an isotropic harmonic potential of frequency ω. At small values of ω, the electrons are strongly correlated. At large values of ω, they are tightly bound. The exact ground state solutions for the Hooke's atom are known for special values of ω.[127,128] We consider here the first nine values of ω for which an analytical solution is available from $\omega = 0.25$ (strongly bound electrons) to $\omega = 3.597 \times 10^{-6}$ (strongly correlated electrons).

The MARE, with respect to the exact von Weizsäcker values ($(T_s^{\mathrm{approx}} - T_s^{\mathrm{W}})/T_s^{\mathrm{W}} \times 100$), are reported in Table 2. The best Laplacian-level meta-GGA results are obtained with MGE4, MGGA, and L0.6, which are also superior to the best GGAs.

In Figure 3, we report the individual deviations for the smallest values of the classical electron distance[127] $r_0 = (\omega^2/2)^{-1/3}$.

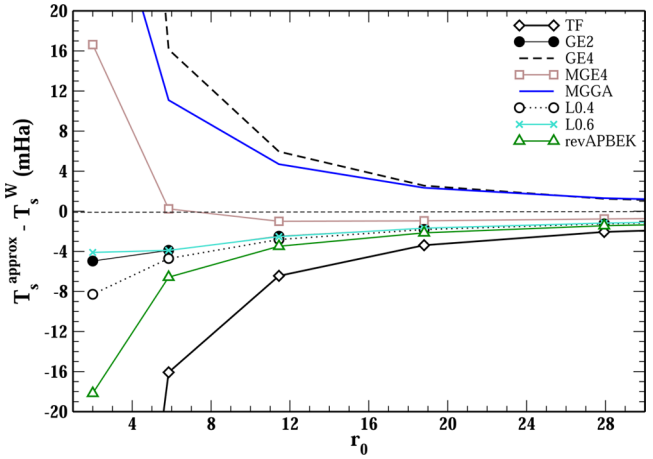

Figure 3. Kinetic energy deviations from the exact values of several KE functionals versus the classical electron distance in the Hooke atom. The von Weizsäcker KE functional is the exact reference for a two-electron closed-shell system.

The L0.4 and L0.6 functionals provide the best description over the whole range of frequencies, whereas the good performance of MGE4 originates from a high accuracy in the strongly correlated regime, while in the tightly bound regime much larger errors are found.

5.3. Jellium Clusters. The KE MAREs for jellium clusters are reported in Table 2. The best Laplacian-level meta-GGA functional is L0.4, the worst is MGGA.

The errors on the kinetic energy per electron ($\Delta T_s/N = (T_s^{\mathrm{approx}}(N) - T_s^{\mathrm{exact}}(N))/N$) for the different clusters are reported in Figure 4 for some selected KE functionals (TF, GE2, GE4, MGE4, MGGA, L0.4); for other functionals, see Figure S9 of the Supporting Information. The data in Figure 4 show that almost of all functionals (but MGGA and TF) work very well for medium and large clusters (i.e., for $N \geq 18$, the error is below 1 mHa), whereas for smaller clusters, definitely larger errors are found. On the other hand, the TF functional yields always an underestimation of the kinetic energy, less dependent on the cluster's size, whereas the MGGA functional shows strong oscillations. In Figure 4, it is worth noting the very close performances of GE2 and L0.4 for all N, despite these two functionals are quite different from each other (Figure 1). This small difference originates from an error cancellation between the region inside the cluster ($s < 1$ and $|q| < 1$, see Figure S10 of the Supporting Information), where L0.4 is (by construction) almost the same as GE4 and thus larger than GE2, and the region outside the cluster (s and q are large), where GE2 is larger than L0.4, as the former diverges with s while the latter approaches a constant (see eq 19).

The dependence of the KE errors on the clusters' size suggests that interesting results may be obtained for the cluster disintegration problem. We consider the disintegration of the cluster with $N = 106$ into smaller magic clusters. The energy

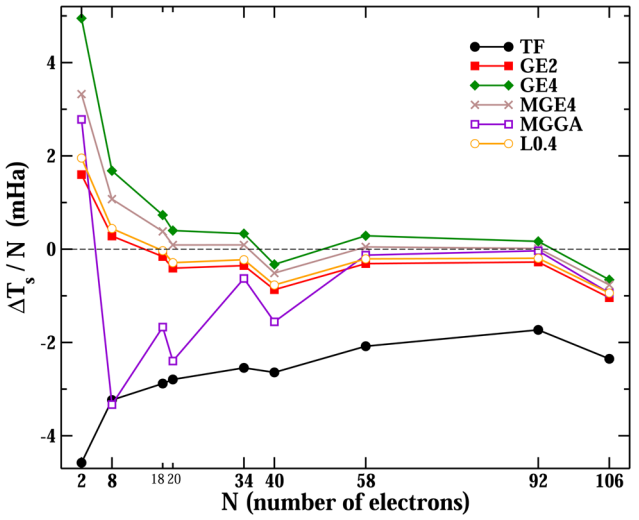

Figure 4. Error on the kinetic energy per electron of the jellium clusters with different electron numbers.

associated with this process is called disintegration kinetic energy (DKE) and is defined as[56] DKE = $\sum_i m_i T_s(N_i) - T_s(106)$, with m_i positive integers such that $\sum_i m_i N_i = 106$ (273 such processes are considered here). If we define $\overline{T}_s(N) = T_s(N)/N$, it is easy to show that DKE = $\sum_i m_i N_i[\overline{T}_s(N_i) - \overline{T}_s(106)]$, which shows that the errors on the DKE are obtained as weighted sums of the differences $\overline{T}_s(N_i) - \overline{T}_s(106)$.

The DKE MARE are reported in Table 2. It turns out that the best Laplacian-level meta-GGA functional is MGGA, which was the worst for the KE. This traces back to the strong oscillations that provide a significant error cancellation. The best overall functional is the TF functional (MARE 17.7), thanks to its almost uniform error among different cluster sizes (despite it is the worst for KE, with MARE 4.4).

5.4. Jellium Surfaces and Slabs. The LDM MAREs[64] of several jellium surfaces are reported in Table 2. The best results are found for GE4, and in general, all Laplacian-level meta-GGA functionals (recovering GE4) overcome the best GGAs. In fact the uniform electron gas scaling becomes important in these systems.

We also calculated the KE energy of two interacting jellium slabs for various distances $0 \le z \le \lambda_F$ between the slabs. The MARE represents $(1/\lambda_F)\int_0^{\lambda_F} dz|T_s(z) - T_s^{exact}(z)|/T_s^{exact}(z)$ and is reported in Table 2 for each functional. Table 2 shows that GE4 and all the Laplacian-level meta-GGA functionals are significantly better than GGAs.

Finally, we also consider the following KE difference DKE = $(1/\lambda_F)\int_0^{\lambda_F} dz[|T_s(z) - T_s(0)| - |T_s^{exact}(z) - T_s^{exact}(0)|]/|T_s^{exact}(z) - T_s^{exact}(0)|$, which represents the dissociation KE of a jellium slab into two pieces and can be used as an indicator of the quality of the functionals in describing bonding regions. Also, in this case, Table 2 shows that Laplacian-level meta-GGA functionals (GE4, L0.4, and L0.6) are significantly better than GGAs.

5.5. Atoms, Ions, and Molecules. The KE MAREs of a benchmark set of atoms and ions are reported in Table 2. The GGAs yield a MARE of about 1%, whereas all the Laplacian-level meta-GGAs are about twice as bad, with a MARE in the range 1.4−2.5%.

As an additional test, we considered the ionization kinetic energies (IKE = $T_s^{atom} - T_s^{ion}$) of the noble gases (until Uuo). Note that because of the virial theorem, IKEs are just equal to the regular ionization potentials. The MARE IKEs are reported in Table 2. All the Laplacian-level meta-GGA functionals (but MGGA) are better than the GGAs. This result traces back to the fact that the GE4-based functionals behave better than GGAs for the homogeneous and fractional scalings and thus for systems with fluctuating number of electrons.

Then, we considered the total and atomization KEs (AKEs) of a set of molecules. We recall that the latter is a hard test for any kinetic energy functional and that most of the functionals even fail to yield a qualitative description of AKEs.[55] Laplacian-level meta-GGA functionals show a MARE for the total KEs below or close to 1%,[66] which is close to the GE2 one but much worse than the best GGA. For the AKE, the trend is similar to the disintegration of the $106\epsilon^-$ jellium cluster.

5.6. Summary and Overall Assessment. Table 2 reports the global MARE (relative to GE2) for the total KE and the KE differences. Concerning the total KE, the best Laplacian-level meta-GGA functional is L0.4, followed by L0.6. Both functionals are largely better than GE4 (MARE reduced to one-half) but are a little worse than the GGA functionals. However, when KE differences are considered, the best performance is yield by the MGGA functional, which definitely overcomes the best GGA. The other Laplacian-level meta-GGA functionals also show very good performances for the KE difference, with MARE(GE2) in the range 0.93−0.96 close to the best GGA.

These results show that in general the inclusion of the Laplacian can improve the description of the noninteracting kinetic energy. However, the proper dependence on this parameter is not captured in a systematic way by any of the functionals that we examined here. As a result, the Laplacian-level meta-GGA functionals perform in a rather random way overcoming the GGAs for some properties and systems but also showing sudden failures for other cases. Anyway, the results summarized in Table 2 indicate that the L0.4 (and L0.6) functional have a more regular behavior than other Laplacian-level meta-GGAs and can be competitive in numerous applications.

6. FDE CALCULATIONS

In this section, we present the results of FDE calculations on different test systems using the Laplacian-level meta-GGA functionals considered in this paper, except GE4, which gives very poor results, even failing to converge in some cases, possibly due to its wrong tail behavior.

6.1. Embedding Densities. The errors on embedding densities (see eq 32) are reported in Table 3. We recall that this is an important test for embedding approaches because it provides direct insight into the quality of the embedding potential.[64,89,90,129−133]

Inspection of the data shows that the L0.4 and L0.6 functionals perform very similarly and are in line with the GGA functionals. On the other hand, MGE4 and MGGA provide significantly larger errors. For weakly interacting systems, both functionals display a very poor performance and interestingly almost the same results. This finding is rationalized considering that for dispersion-dominated systems the bond region is characterized by small and medium values of s and quite large values of q ($q \gtrsim 5$). Thus, in this region, the two functionals and the corresponding kinetic potentials are the same by construction (in this region $F_s^{MGE4} > F_s^{W}$, hence $F_s^{MGGA} = F_s^{MGE4}$; see eqs 12 and 13 as well as the plots of the enhancement factor reported in the Supporting Information). On the other hand, for the other kinds of interactions, only MGGA shows a poor

Table 3. Global Absolute Errors on Embedding Densities (eq 32), Resulting from FDE Calculations with Different KE Functionals on Several Classes of Systems (Weak, Dipole−Dipole, and Hydrogen-Bonded Systems)[a]

	GGAs				meta-GGAs			
system	TF	GE2	APBEK	revAPBEK	MGE4	MGGA	L0.4	L0.6
Weak interaction								
He−Ne	0.71	0.93	0.71	0.70	1.46	1.53	**0.76**	**0.76**
He−Ar	0.78	1.16	0.78	0.78	1.88	2.01	0.85	**0.83**
Ne−Ne	0.17	0.50	0.12	0.08	1.58	1.58	0.26	**0.21**
Ne−Ar	0.22	0.65	0.14	0.10	2.02	2.02	0.31	**0.19**
CH_4−Ne	0.28	0.75	0.17	0.12	2.54	2.53	0.39	**0.29**
C_6H_6−Ne	0.41	0.64	0.19	0.18	2.32	2.32	0.38	**0.21**
CH_4−CH_4	0.59	1.39	0.29	0.60	5.89	5.64	**0.36**	0.77
MAE	0.45	0.86	0.34	0.37	2.53	2.52	**0.47**	**0.47**
Dipole−dipole interaction								
H_2S−H_2S	2.19	2.29	2.01	2.08	**2.17**	4.67	2.73	2.86
HCl−HCl	2.70	2.60	2.47	2.50	**2.54**	4.56	2.76	2.86
H_2S−HCl	5.07	4.64	4.79	4.78	**4.17**	6.59	4.73	4.77
CH_3Cl−HCl	3.35	3.25	3.04	3.08	4.07	5.35	**3.15**	3.28
CH_3SH−HCN	1.86	2.29	1.91	2.05	3.26	5.08	**2.56**	2.68
CH_3SH−HCl	5.47	5.22	5.22	5.24	5.71	6.60	**5.13**	5.15
MAE	3.44	3.38	3.24	3.29	3.65	5.47	**3.51**	3.60
Hydrogen bond interaction								
NH_3−NH_3	2.32	2.30	2.04	2.12	**2.50**	5.44	2.92	2.91
HCl-HCl	2.69	2.38	2.22	2.19	**2.28**	5.36	2.35	2.36
H_2O−H_2O	2.94	2.73	2.55	2.58	**2.67**	6.02	3.02	2.96
NH_3−H_2O	4.57	4.14	4.26	4.26	**4.04**	7.38	4.52	4.47
HF-NCH	4.49	4.22	4.22	4.22	**4.09**	6.80	4.29	4.25
$(HCONH_2)_2$	3.17	3.32	3.17	3.30	∗**3.13**	6.78	3.92	3.78
$(HCOOH)_2$	4.84	4.54	4.65	4.69	∗**4.03**	6.85	4.82	4.69
MAE	3.57	3.38	3.30	3.34	∗**3.25**	6.38	3.69	3.63
Overall assessment								
MAE	1.81	1.85	1.66	1.69	2.31	3.52	**1.86**	**1.86**

[a]The mean absolute error (MAE) for each set of molecules and the total MAE are also reported. The best (worst) Laplacian-level meta-GGA value on each line is highlighted in bold (underline) style. The star symbol stands for a Laplacian-level meta-GGA KE functional that is better than the best GGA.

behavior, whereas MGE4 performs rather well, being even the best Laplacian-level meta-GGA for hydrogen bonds. In this case in fact the bonding region is characterized by small and medium values of s but small values of q ($q \sim 0.5$) so that MGE4 recovers GE4, which is a reasonable limit. However, this is exactly the range of values where the sharp interpolating function of MGGA assumes its intermediate values. Therefore, the MGGA potential is strongly oscillating in this region (Figure 1).

To understand better these results, we consider in Figure 5, the plot of the plane-averaged deformation density in two typical cases: for the hydrogen bond complex HF−NCH and for the weakly interacting Ne−Ar system. The figure confirms the findings of Table 3 and additionally indicates that the GGA and L0.4/L0.6 densities are in fact similar over the whole space (not only after integration). On the contrary, MGE4 is very similar to L0.4 for hydrogen bond complexes but almost identical to MGGA for weakly interacting complexes. Note that the HF−NCH complex has larger density in the bond than Ne−Ar; thus, the relative errors in the bond are larger in the latter case that in the former.

6.2. Embedding Energies. The errors on the embedding energies obtained from FDE calculations using different kinetic functionals are reported in Table 4. The data show that the L0.4 functional has MAE = 1.06 mHa, which is comparable to that of the state-of-the-art GGA KE functionals and lower than the errors originating from the XC approximation.[124] In particular, L0.4 yields the best results (MAE = 0.64 mHa) for the dipole−dipole interaction systems, also outperforming revAPBEK. On the other hand, lower accuracy is obtained for the weakly interacting systems. This drawback can be related to the inaccuracy of the gradient expansion for this class of systems, as it will be explained below (see next section). In general, we can state the important result that the L0.4 Laplacian-level functional can be effectively used to approximate the nonadditive kinetic energy functional in embedding calculations, yielding accurate total embedding energies for noncovalently interacting systems.

Concerning the other Laplacian-level meta-GGA functionals, slightly worse results are found with L0.6, which gives in any case rather good results, in line with APBEK. For the MGE4 and MGGA functionals, similar considerations as for the case of the embedding densities apply. In fact, as shown in more details in next section, for weakly interacting systems, the embedding energy is mainly determined by the region having moderately large s values and large values of the reduced Laplacian ($q \gtrsim 5$). Hence, the two functionals perform very similarly and yield strongly underestimated embedding energies (see next section). For dipole−dipole and hydrogen bond interactions, instead the relevant region for the embedding energy is defined (see next section) by relatively small values of the reduced parameters ($s \lesssim 1$ and $|q| \lesssim 1$). Thus, MGE4 correctly tends to GE4, which is a rather good approximation for this limit,

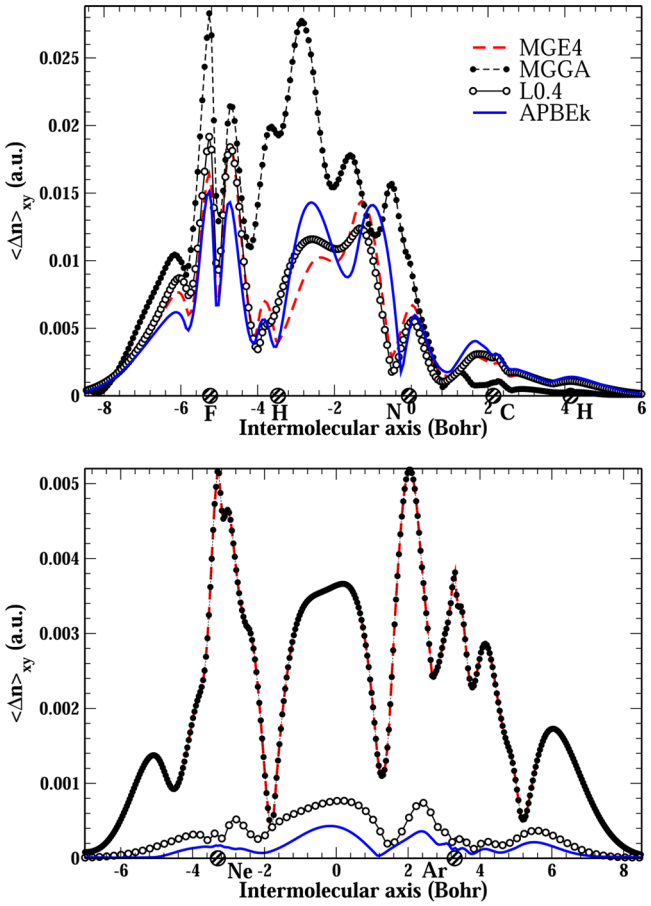

Figure 5. Plane-averaged deformation densities obtained from different KE functionals for the HF−NCH hydrogen bond complex (upper panel) and the weakly interacting Ne−Ar dimer. The filled circles on the x axis denote the atoms' positions.

whereas MGGA is dominated by the interpolating function (see the plot of the enhancement factor in the Supporting Information).

6.3. Energy Decomposition Analysis. To analyze in more details Laplacian-level kinetic energy functionals, we extend the idea proposed in ref 64. Thus, we perform a decomposition of the nonadditive KE in terms of the reduced gradient and Laplacian contributions. Similarly with the GGA case,[64] we define the following transformation of the Thomas−Fermi kinetic energy density

$$t[n](s,q) = \int \tau^{\mathrm{TF}}[n](\mathbf{r})\delta(s - s(\mathbf{r}))\delta(q - q(\mathbf{r}))\mathrm{d}\mathbf{r} \tag{35}$$

so that the Thomas−Fermi kinetic energy is

$$T_s^{\mathrm{TF}}[n] = \int\int t[n](s,q)\mathrm{d}s\mathrm{d}q \tag{36}$$

where $t[n](s,q)$ is the (s,q)-decomposed homogeneous electron gas (HEG) KE distribution. For a Laplacian-level meta-GGA KE functional we have

$$T_s[F_s,n] = \int\int t[n](s,q)F_s(s,q)\mathrm{d}s\mathrm{d}q \tag{37}$$

Equation 37 states that the total kinetic energy is the scalar product (in the (s,q) space) of $t(s,q)$ and the kinetic enhancement factor $F_s(s,q)$. Thus, in this formalism, T_s is also a functional of F_s. Then, as the definition of the nonadditive kinetic energy is linear in the composing total KEs (eq 3), we also obtain

$$T_s^{\mathrm{nadd}}[F_s;n_A;n_B] = \int\int t^{\mathrm{nadd}}[n_A;n_B](s,q)F_s(s,q)\mathrm{d}s\mathrm{d}q \tag{38}$$

with

$$t^{\mathrm{nadd}}[n_A;n_B](s,q) = t[n_A + n_B](s,q) - t[n_A](s,q) - t[n_B](s,q) \tag{39}$$

Equation 39 is a generalization of eq 19 of ref 64. Note that the (s,q) decomposition is a more powerful tool as compared to the s decomposition because the former can distinguish important density regions, such as $s \approx 0$, $q > 0$ in the bond, and $s \leq 0.4$, $q < 0$ near the nucleus, which cannot be resolved in the s-only decomposition.

Following ref 64, we thus have that the embedding energy error for given approximated embedded density can be written as

$$\Delta E[F_s] \approx \int\int t^{\mathrm{nadd}}[n_A;n_B](s,q)F_s(s,q)\mathrm{d}s\mathrm{d}q + \Delta W \tag{40}$$

where ΔW is a constant, i.e., a known bifunctional of the embedded densities.

We note that if a GGA enhancement factor is considered using $\int_{-\infty}^{\infty}\mathrm{d}x\ \delta(x) = 1$, eq 40 correctly turns into the GGA expression

$$\Delta E[F_s] \approx \int F_s(s)\left[\int t^{\mathrm{nadd}}[n_A;n_B](s,q)\mathrm{d}q\right]\mathrm{d}s + \Delta W = \int F_s(s)\langle t^{\mathrm{nadd}}[n_A;n_B]\rangle_q(s)\mathrm{d}s + \Delta W \tag{41}$$

i.e., the q-averaged integral nonadditive s,q-decomposed HEG kinetic energy distribution $\langle t^{\mathrm{nadd}}[n_A;n_B]\rangle_q(s)$ corresponds to the nonadditive HEG kinetic energy distribution obtained in ref 64 for the s decomposition of a GGA functional (eqs 14 and 19 of ref 64).

Equation 40 can be used to understand the role of $F_s(s,q)$ and the performance of different Laplacian-level meta-GGAs in terms of the shape of their enhancement factor in the (s,q) space.

As an application of the present (s,q) decomposition, we consider the HF−NCH and Ne_2 complexes. The L0.4 functional gives almost the exact energy for the former (embedding error of only 0.17mHa), whereas it is quite inaccurate for the latter (embedding error larger than the binding energy). Figure 6 reports, for the two systems, the nonadditive (s,q)-decomposed HEG kinetic energy distribution $t^{\mathrm{nadd}}(s,q)$ (upper panel), as well as the plot of $\langle t^{\mathrm{nadd}}\rangle_q(s)$ (lower panel), both calculated by fixing the embedded densities to the APBEK ones. Integration in eq 35 was performed numerically, representing the delta function with a Gaussian model with broadening $\sigma = 0.07$.

The plots on the bottom panels show that in analogy with the GGA case studied in ref 64 the correct embedding energy comes from a delicate balancing of positive contributions at small s values and negative contributions at larger values of s in the scalar product (eq 38). On the other hand, richer structures are present considering $t^{\mathrm{nadd}}(s,q)$ and several considerations can be done:

(i) Contributions from negative q are negligible, meaning that the core regions are not important for $t^{\mathrm{nadd}}(s,q)$. This information cannot be extracted from the s-only decomposition

Table 4. Embedding Energy Errors (eq 29) in mHa Resulting from FDE Calculations with Different KE Functionals on Several Classes of Systems (Weak, Dipole−Dipole, and Hydrogen-Bonded Systems)[a]

		GGAs				meta-GGAs			
system	E_b	TF	GE2	APBEK	revAPBEK	MGE4	MGGA	L0.4	L0.6
Weak interaction									
He−Ne	0.06	0.38	−0.81	0.39	0.35	-3.28	−3.24	**0.48**	0.50
He−Ar	0.10	0.43	−0.81	0.44	0.40	−3.20	−3.13	**0.55**	0.57
Ne−Ne	0.13	0.29	−1.67	0.27	0.18	−4.45	−4.45	**0.50**	0.52
Ne−Ar	0.21	0.34	−1.84	0.29	0.16	−4.44	−4.44	**0.57**	**0.57**
CH_4−Ne	0.35	0.37	−2.05	0.32	0.18	−7.11	−7.11	**0.63**	0.64
C_6H_6−Ne	0.75	1.05	−4.49	0.61	0.14	−13.39	−13.39	1.59	**1.45**
CH_4−CH_4	0.81	0.78	−4.39	0.21	−0.29	−13.29	−13.13	1.05	**0.67**
MAE		0.52	2.29	0.36	0.24	7.02	6.98	0.77	**0.70**
Dipole−dipole interaction									
H_2S−H_2S	2.63	2.15	−4.68	0.67	−0.23	−3.83	−7.80	∗**−0.04**	−1.19
HCl−HCl	3.20	3.26	−4.76	1.49	0.44	−3.67	−8.76	0.73	**0.60**
H_2S−HCl	5.34	5.28	−4.83	2.46	1.05	−3.91	−12.55	∗**0.44**	∗−1.03
CH_3Cl−HCl	5.66	5.92	−7.08	2.42	0.63	−7.37	−15.40	1.12	**−0.82**
CH_3SH-HCN	5.72	2.79	−7.34	0.53	−0.79	−9.84	−16.55	∗**−0.24**	−1.78
CH_3SH−HCl	6.63	8.46	−6.30	3.80	1.72	−7.23	−19.07	∗1.24	∗**−0.65**
MAE		4.64	5.83	1.90	0.81	5.97	13.36	∗**0.64**	1.01
Hydrogen bond interaction									
NH_3−NH_3	5.02	2.63	−6.20	0.63	−0.55	−5.21	−11.44	∗**−0.50**	−1.94
HCl−HCl	7.28	5.23	−5.87	2.77	1.29	−4.21	−15.32	1.42	**−0.49**
H_2O−H_2O	7.92	4.77	−6.82	1.84	0.24	−5.42	−16.22	∗**−0.17**	−1.93
NH_3−H_2O	10.21	5.97	−6.98	2.17	0.34	−6.28	−19.97	**−0.86**	−2.65
HF−NCH	11.33	8.26	−6.62	3.78	1.67	−5.85	−23.46	∗**0.17**	−1.89
$(HCONH_2)_2$	23.81	10.59	−17.72	1.43	−2.76	−17.85	−52.06	**−5.42**	−9.11
$(HCOOH)_2$	25.74	18.81	−15.77	6.13	0.99	−15.49	−60.77	**−3.49**	−7.26
MAE		8.04	9.43	2.68	1.12	8.62	28.46	**1.72**	3.61
Overall assessment									
MAE		4.39	5.85	1.63	0.72	7.27	16.41	**1.06**	1.81

[a]The second column reports the benchmark binding energy $E_b$from ref 124. The mean error (ME), mean absolute error (MAE), and the mean absolute relative error (MARE) are indicated for each set of molecules. At the bottom of the table, the total MAEs are also reported. The best (worst) Laplacian-level meta-GGA value on each line is highlighted in bold (underline) style. The star symbol stands for a Laplacian-level meta-GGA KE functional that is better than the best GGA.

because both the core region as well as the valence region have $s \lesssim 0.4$.

(ii) For HF−NCH, the q dependence of $t^{nadd}(s,q)$ is quite weak, explaining the success of GGA approximations, which rely on the q-averaged integral of $t^{nadd}(s,q)$. Moreover, the nonzero values of $t^{nadd}(s,q)$ are mostly confined in the range of $0 \le q \le 2$ and $0 \le s \le 2$, which is related to the bonding region (the value of q at the center of the bond is $q \approx 0.5$). In this region of the (s,q)-space (small s and small q), the fourth-order gradient expansion can be correct, explaining the very low embedding errors of L0.4 (which recovers GE4). Similar plots have been obtained for other hydrogen bond or dipole−dipole interaction systems and are reported in the Supporting Information.

(iii) For Ne_2, the $t^{nadd}(s,q)$ looks very different. The most important structures are now at $s > 1.5$ and $4 \le q \le 8$. In fact, due to the weakly interacting character of the system, the value of the reduced Laplacian at the center of the bond is $q \approx 6.8$. The plot thus shows how difficult can be the construction of an accurate Laplacian-level kinetic functional for FDE. In fact, the embedding energy error depends on the product over the whole (s,q) space of $t^{nadd}(s,q)$ and the kinetic enhancement factor $F_s(s,q)$. Hence, an accurate enhancement factor should properly take into account the complexity of the structures at $4 \le q \le 8$ and $s > 1.5$. However, the L0.4/L0.6 enhancement factor is only weakly dependent on q for $s > 3$ (see plots S7 and S8 in the Supporting Information). On the other hand, GGA functionals average over q and loose all q-dependent structures; nevertheless, they can still be very accurate for weakly interaction systems (see, e.g., revAPBEK) thanks to an error cancellation in different q regions. This error cancellation is however less likely (and also undesired) for Laplacian-level kinetic functionals.

Finally, the plot of Figure 6 also explains the fact that MGGA and MGE4 always yield strongly underestimated embedding energies. This fact traces back to the diverging enhancement factor as s increases (Figure 1). This *exact* feature brings an overestimation of the negative contributions of $t^{nadd}(s,q)$ (always located at large s values), which is not well balanced by the regions responsible for the positive contributions. Thus, too negative embedding energies (even more negative than for GE2) are obtained.

7. CONCLUSIONS

In this work we investigated the significance of the fourth-order gradient expansion of the kinetic energy. To this end, we performed a thorough assessment of several Laplacian-level meta-GGA kinetic energy functionals, with special attention to subsystem DFT applications.

Our study indicated that the inclusion of information coming from the Laplacian of the density into the functional may play an important role toward higher accuracy and broader applicability. In fact, GE4 significantly improves over GE2 for

dx.doi.org/10.1021/ct400836s | J. Chem. Theory Comput. 2014, 10, 164−179

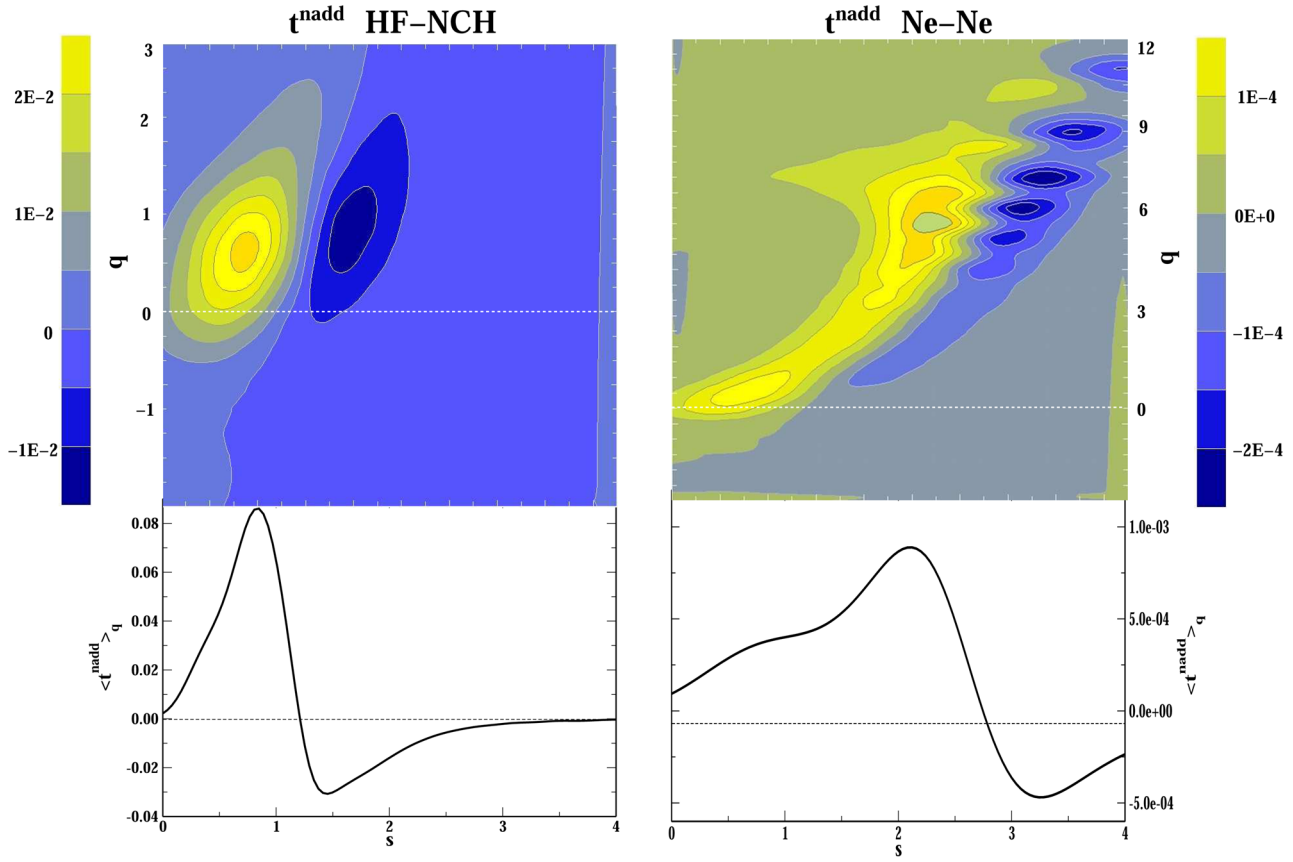

Figure 6. (s,q)-decomposed nonadditive HEG kinetic energy distribution ($t^{\mathrm{nadd}}(s,q)$) for the complex HF–NCH (left) and for Ne_2 (right), with s and q in the range appropriate to physical densities. The corresponding q-averaged integral of $t^{\mathrm{nadd}}(s,q)$ ($\langle t^{\mathrm{nadd}}\rangle_q(s)$) is also reported for comparison in the bottom panels.

solid-state related models (as jellium surfaces, interacting jellium slabs, and large jellium clusters; Table 2), as well as for the monovacancy formation in jellium.[134] Nevertheless, GE4 shows serious drawbacks for small finite systems (e.g., light atoms) due to a nonphysical behavior near the nucleus and in the tail of the density, which make the construction of GE4-based functionals a real challenge. In fact, the different Laplacian-level meta-GGAs tested in this paper displayed a quite disappointing unsystematic accuracy being quite good for some properties and systems and rather poor (at least worse than GGA methods) for others. These problems become especially evident in FDE applications, where the quality of the nonadditive kinetic potential plays a fundamental role, being applied to different densities at the same time. In fact, most of the Laplacian-level meta-GGA functionals considered in the present study perform poorly, and several also yield severe convergence problems.

The notable exception to this behavior is given by the L0.4 and L0.6 functionals, which perform overall rather close to the best GGAs, especially in embedding calculations of small molecular complexes, while being better than the best GGAs for solid-state related jellium models. The reason for this traces back to the fact that these functionals were constructed not only to recover GE4 in the slowly varying density limit but also to achieve reasonably good behavior in the rapidly varying regime. This later goal was obtained by mimicking the successful behavior of the revAPBEK functional in the rapidly varying limit. Thus, the L0.4 and L0.6 functionals appear as promising tools for the application of Laplacian-level meta-GGA kinetic energy functionals in the context of FDE or the density-decomposed orbital-free DFT.[77,78]

We remark, however, that the main message emerging from the present work is that there is still a huge amount of work to be done in the development of Laplacian-level meta-GGA kinetic energy functionals before they can significantly overcome the more simple GGAs for FDE applications to weakly interacting systems. This future work should be focused on studying in deeper details the role played by the Laplacian in different systems and density regimes, so that more complex dependences on the q variable can be developed, especially in the rapidly varying density regime. In fact, with our assessment work, and in particular through the (s,q) decomposition technique, we showed that the actual Laplacian-level meta-GGA functionals display a reliable q-dependence only in the slowly varying limit, whereas they show limitations in the rapidly varying regions.

THE IMPLEMENTATION OF LAPLACIAN-LEVEL META-GGAs

For any Laplacian level DFT functional of the form

$$T_s[n] = \int \tau_s[n, \nabla n, \nabla^2 n](\mathbf{r})\mathrm{d}\mathbf{r} \tag{42}$$

the functional derivative with respect to the electron density is

$$\frac{\delta T_s[n]}{\delta n(\mathbf{r})} = \frac{\partial \tau_s[n](\mathbf{r})}{\partial n(\mathbf{r})} - \nabla\cdot\frac{\partial \tau_s[n](\mathbf{r})}{\partial \nabla n(\mathbf{r})} + \nabla^2\frac{\partial \tau_s[n](\mathbf{r})}{\partial \nabla^2 n(\mathbf{r})} \tag{43}$$

dx.doi.org/10.1021/ct400836s | J. Chem. Theory Comput. 2014, 10, 164–179

The matrix elements between the basis set functions $\{\chi_i\}$ required in FDE calculations are therefore

$$
\begin{aligned}
(v_s)_{\mu\nu} &= \int \chi_\mu(\mathbf{r}) \frac{\delta T[n]}{\delta n(\mathbf{r})} \chi_\nu(\mathbf{r}) \mathrm{d}\mathbf{r} \\
&= \int \chi_\mu(\mathbf{r}) \frac{\partial \tau_s[n](\mathbf{r})}{\partial n(\mathbf{r})}(\mathbf{r}) \chi_\nu(\mathbf{r}) \mathrm{d}\mathbf{r} \\
&+ \int \frac{\partial \tau_s[n](\mathbf{r})}{\partial \nabla n}(\mathbf{r}) \cdot [\nabla \chi_\mu(\mathbf{r}) \chi_\nu(\mathbf{r}) + \nabla \chi_\nu(\mathbf{r}) \chi_\mu(\mathbf{r})] \mathrm{d}\mathbf{r} \\
&+ \int \frac{\partial \tau_s[n](\mathbf{r})}{\partial \nabla^2 n(\mathbf{r})}(\mathbf{r}) [\nabla^2 \chi_\mu(\mathbf{r}) \chi_\nu(\mathbf{r}) + 2 \nabla \chi_\mu(\mathbf{r}) \cdot \nabla \chi_\nu(\mathbf{r}) \\
&+ \chi_\mu(\mathbf{r}) \nabla^2 \chi_\nu(\mathbf{r})] \mathrm{d}\mathbf{r}
\end{aligned} \tag{44}
$$

where we used the first $\left(\int f(\mathbf{r}) \nabla \cdot \mathbf{v}(\mathbf{r}) \mathrm{d}\mathbf{r} = -\int \nabla f(\mathbf{r}) \cdot \mathbf{v}(\mathbf{r}) \mathrm{d}\mathbf{r}\right)$ and the second Green's identities $\left(\int f(\mathbf{r}) \nabla^2 g(\mathbf{r}) \mathrm{d}\mathbf{r} = \int \nabla^2 f(\mathbf{r}) g(\mathbf{r}) \mathrm{d}\mathbf{r}\right)$.

■ ASSOCIATED CONTENT

Supporting Information

Plots of the enhancement factors, plots of jellium clusters KE and reduced gradients, results of supermolecular FDE calculations, and additional plots for the (s,q)-decomposition of the nonadditive KE. This material is available free of charge via the Internet at http://pubs.acs.org.

■ AUTHOR INFORMATION

Corresponding Author

*E-mail: lucian.constantin@iit.it.

Notes

The authors declare no competing financial interest.

■ ACKNOWLEDGMENTS

This work was partially funded by the European Research Council (ERC) Starting Grant FP7 Project DEDOM, Grant No. 207441. The authors thank TURBOMOLE GmbH for providing the TURBOMOLE program package and M. Margarito for technical support.

■ REFERENCES

(1) Thomas, L. H. The calculations of atomic fields. *Proc. Cambridge Phil. Soc.* **1926**, *23*, 542.
(2) Fermi, E. Un metodo statistico per la determinazione di alcune proprieta' dell'atomo. *Rend. Accad. Naz. Lincei* **1927**, *6*, 602.
(3) Fermi, E. A statistical method for the determination of some atomic properties and the application of this method to the theory of the periodic system of elements. *Z. Phys.* **1928**, *48*, 73.
(4) Parr, R. G.; Yang, W. *Density-Functional Theory of Atoms and Molecules*; Oxford University Press: Oxford, 1989.
(5) Dreizler, R. M.; Gross, E. K. U. *Density Functional Theory*; Springer: Heidelberg, 1990.
(6) Lignères, V. L.; Carter, E. A. *Handbook of Materials Modeling*; Springer Science and Business Media: Dordrecht, The Netherlands, 2005; pp 137−148.
(7) Chen, H.; Zhou, A. Orbital-free density functional theory for molecular structure calculations. *Numer. Math. Theory Meth. Appl.* **2008**, *1*, 1−28.
(8) von Weizsäcker, C. F. Zur theorie der Kernmassen. *Z. Phys. A* **1935**, *96*, 431−458.
(9) Kirzhnitz, D. Quantum corrections to the Thomas−Fermi equation. *Sov. Phys. JETP* **1957**, *5*, 64.
(10) Yonei, K.; Tomishima, Y. On the Weizsäcker correction to the Thomas−Fermi theory of the atom. *J. Phys. Soc. Jpn.* **1965**, *20*, 1051.
(11) Oliver, G. L.; Perdew, J. P. Spin-density gradient expansion for the kinetic energy. *Phys. Rev. A* **1979**, *20*, 397−403.
(12) Murphy, D. R. Sixth-order term of the gradient expansion of the kinetic-energy density functional. *Phys. Rev. A* **1981**, *24*, 1682−1688.
(13) Wigner, E. On the quantum correction for thermodynamic equilibrium. *Phys. Rev.* **1932**, *40*, 749−759.
(14) Kirkwood, J. G. Quantum statistics of almost classical assemblies. *Phys. Rev.* **1933**, *44*, 31−37.
(15) Brack, M.; Jennings, B. K.; Chu, Y. H. On the extended Thomas−Fermi approximation to the kinetic energy density. *Phys. Lett. B* **1976**, *65*, 1−4.
(16) March, N. H. Partial summation of gradient expansion of canonical density matrix. *Phys. Lett. A* **1977**, *64*, 185−186.
(17) Jennings, B. K. The extended Thomas−Fermi density matrix. *Phys. Lett. B* **1978**, *74*, 13−14.
(18) Engel, E.; Dreizler, R. M. Extension of the Thomas−Fermi−Dirac−Weizsäcker model: Four-order gradient corrections to the kinetic energy. *J. Phys. B* **1989**, *22*, 1901.
(19) Yang, W. Gradient correction in Thomas−Fermi theory. *Phys. Rev. A* **1986**, *34*, 4575−4585.
(20) Scott, J. The binding energy of the Thomas−Fermiatom. *Philos. Mag.* **1952**, *43*, 859.
(21) Golden, S. Statistical theory of many-electron systems. General considerations pertaining to the Thomas−Fermi theory. *Phys. Rev.* **1957**, *105*, 604−615.
(22) Jones, W.; Young, W. H. Density functional theory and the von Weizsäcker method. *J. Phys. C* **1971**, *4*, 1322.
(23) Hodges, C. H. Quantum corrections to the Thomas−Fermi approximation: The Kirzhnits method. *Can. J. Phys.* **1973**, *51*, 1428.
(24) Wang, L.-W.; Teter, M. P. Kinetic-energy functional of the electron density. *Phys. Rev. B* **1992**, *45*, 13196−13220.
(25) Levy, M.; Ou-Yang, H. Exact properties of the Pauli potential for the square root of the electron density and the kinetic energy functional. *Phys. Rev. A* **1988**, *38*, 625−629.
(26) Bartolotti, L. J.; Acharya, P. K. On the functional derivative of the kinetic energy density functional. *J. Chem. Phys.* **1982**, *77*, 4576−4585.
(27) Yang, W.; Parr, R. G.; Lee, C. Various functionals for the kinetic energy density of an atom or molecule. *Phys. Rev. A* **1986**, *34*, 4586−4590.
(28) Karasiev, V. V.; Ludeña, E. V.; Artemyev, A. N. Electronic-structure kinetic-energy functional based on atomic local-scaling transformations. *Phys. Rev. A* **2000**, *62*, 062510.
(29) Pis Diez, R.; Karasiev, V. V. A relationship between the weighted density approximation and the local−scaling transformation version of density functional theory. *J. Phys. B* **2003**, *36*, 2881.
(30) Lee, H.; Lee, C.; Parr, R. G. Conjoint gradient correction to the Hartree−Fock kinetic- and exchange-energy density functionals. *Phys. Rev. A* **1991**, *44*, 768−771.
(31) March, N. H.; Santamaria, R. Non-local relation between kinetic and exchange energy densities in Hartree−Fock theory. *Int. J. Quantum Chem.* **1991**, *39*, 585−592.
(32) Perdew, J. P. Generalized gradient approximation for the fermion kinetic energy as a functional of the density. *Phys. Lett. A* **1992**, *165*, 79−82.
(33) Lacks, D. J.; Gordon, R. G. Tests of nonlocal kinetic energy functionals. *J. Chem. Phys.* **1994**, *100*, 4446−4452.
(34) DePristo, A. E.; Kress, J. D. Kinetic-energy functionals via Padé approximations. *Phys. Rev. A* **1987**, *35*, 438−441.
(35) Thakkar, A. J. Comparison of kinetic-energy density functionals. *Phys. Rev. A* **1992**, *46*, 6920−6924.
(36) Tran, F.; Wesolowski, T. A. Link between the kinetic- and exchange-energy functionals in the generalized gradient approximation. *Int. J. Quantum Chem.* **2002**, *89*, 441.
(37) Karasiev, V. V.; Trickey, S. B.; Harris, F. E. Born−Oppenheimer interatomic forces from simple, local kinetic energy density functionals. *J. Comput.-Aided Mater. Des.* **2006**, *13*, 111.

(38) Karasiev, V. V.; Jones, R. S.; Trickey, S. B.; Harris, F. E. Properties of constraint-based single-point approximate kinetic energy functionals. *Phys. Rev. B* **2009**, *80*, 245120.
(39) Huang, C.; Carter, E. A. Nonlocal orbital-free kinetic energy density functional for semiconductors. *Phys. Rev. B* **2010**, *81*, 045206.
(40) Wang, Y. A.; Govind, N.; Carter, E. A. Orbital-free kinetic-energy functionals for the nearly free electron gas. *Phys. Rev. B* **1998**, *58*, 13465−13471.
(41) Wang, Y. A.; Govind, N.; Carter, E. A. Erratum: Orbital-free kinetic-energy functionals for the nearly free electron gas [*Phys. Rev. B* **1998**, *58*, (13), 465]. *Phys. Rev. B* **2001**, *64*, 129901.
(42) Alonso, J. A.; Girifalco, L. A. Nonlocal approximation to the exchange potential and kinetic energy of an inhomogeneous electron gas. *Phys. Rev. B* **1978**, *17*, 3735−3743.
(43) Chacón, E.; Alvarellos, J. E.; Tarazona, P. Nonlocal kinetic energy functional for nonhomogeneous electron systems. *Phys. Rev. B* **1985**, *32*, 7868−7877.
(44) García-González, P.; Alvarellos, J. E.; Chacón, E. Nonlocal kinetic-energy-density functionals. *Phys. Rev. B* **1996**, *53*, 9509−9512.
(45) García-González, P.; Alvarellos, J. E.; Chacón, E. Kinetic-energy density functional: Atoms and shell structure. *Phys. Rev. A* **1996**, *54*, 1897−1905.
(46) García-González, P.; Alvarellos, J. E.; Chacón, E. Nonlocal symmetrized kinetic-energy density functional: Application to simple surfaces. *Phys. Rev. B* **1998**, *57*, 4857−4862.
(47) García-González, P.; Alvarellos, J. E.; Chacón, E. Kinetic−energy density functionals based on the homogeneous response function applied to one-dimensional fermion systems. *Phys. Rev. A* **1998**, *57*, 4192−4200.
(48) Smargiassi, E.; Madden, P. A. Orbital-free kinetic-energy functionals for first-principles molecular dynamics. *Phys. Rev. B* **1994**, *49*, 5220−5226.
(49) Foley, M.; Madden, P. A. Further orbital-free kinetic-energy functionals for ab initio molecular dynamics. *Phys. Rev. B* **1996**, *53*, 10589−10598.
(50) Wang, Y. A.; Govind, N.; Carter, E. A. Orbital-free kinetic-energy density functionals with a density-dependent kernel. *Phys. Rev. B* **1999**, *60*, 16350−16358.
(51) Karasiev, V. V.; Jones, R. S.; Trickey, S. B.; Harris, F. E. Recent Advances in Developing Orbital-Free Kinetic Energy Functionals. In *New Developments in Quantum Chemistry*; Transworld Research Network: Kerala, India, 1989.
(52) Acharya, P. K.; Bartolotti, L. J.; Sears, S. B.; Parr, R. G. An atomic kinetic energy functional with full Weizsacker correction. *Proc. Natl. Acad. Sci.* **1980**, *77*, 6978−6982.
(53) Ou-Yang, H.; Levy, M. Approximate noninteracting kinetic energy functionals from a nonuniform scaling requirement. *Int. J. Quantum Chem.* **1991**, *40*, 379.
(54) Vitos, L.; Skriver, H. L.; Kollár, J. Kinetic−energy functionals studied by surface calculations. *Phys. Rev. B* **1998**, *57*, 12611−12615.
(55) Perdew, J. P.; Constantin, L. A. Laplacian-level density functionals for the kinetic energy density and exchange−correlation energy. *Phys. Rev. B* **2007**, *75*, 155109.
(56) Constantin, L. A.; Ruzsinszky, A. Kinetic energy density functionals from the airy gas with an application to the atomization kinetic energies of molecules. *Phys. Rev. B* **2009**, *79*, 115117.
(57) García-Aldea, D.; Alvarellos, J. E. Kinetic energy density study of some representative semilocal kinetic energy functionals. *J. Chem. Phys.* **2007**, *127*, 144109.
(58) García-Aldea, D.; Alvarellos, J. E. Fully nonlocal kinetic energy density functionals: A proposal and a general assessment for atomic systems. *J. Chem. Phys.* **2008**, *129*, 074103.
(59) Garca-Aldea, D.; Alvarellos, J. E. Approach to kinetic energy density functionals: Nonlocal terms with the structure of the von Weizsäcker functional. *Phys. Rev. A* **2008**, *77*, 022502.
(60) Chai, J.-D.; Weeks, J. D. Orbital-free density functional theory: Kinetic potentials and ab initio local pseudopotentials. *Phys. Rev. B* **2007**, *75*, 205122.
(61) Lembarki, A.; Chermette, H. Obtaining a gradient-corrected kinetic-energy functional from the Perdew−Wang exchange functional. *Phys. Rev. A* **1994**, *50*, 5328.
(62) Götz, A. W.; Beyhan, S. M.; Visscher, L. Performance of kinetic energy functionals for interaction energies in a subsystem formulation of density functional theory. *J. Chem. Theory Comput.* **2009**, *5*, 3161−3174.
(63) Constantin, L. A.; Fabiano, E.; Laricchia, S.; Della Sala, F. Semiclassical neutral atom as a reference system in density functional theory. *Phys. Rev. Lett.* **2011**, *106*, 186406.
(64) Laricchia, S.; Fabiano, E.; Constantin, L. A.; Della Sala, F. Generalized gradient approximations of the noninteracting kinetic energy from the semiclassical atom theory: Rationalization of the accuracy of the frozen density embedding theory for nonbonded interactions. *J. Chem. Theory Comput.* **2011**, *7*, 2439−2451.
(65) Tran, F.; Wesolowski, T. A. In *Recent Advances in Computational Chemistry 6*; Wesolowski, T. A., Wang, Y. A., Eds.; World Scientific: Singapore, 2013; pp 429−442.
(66) Tran, F.; Wesolowski, T. A. Introduction of the explicit long-range nonlocality as an alternative to the gradient expansion approximation for the kinetic-energy functional. *Chem. Phys. Lett.* **2002**, *360*, 209−216.
(67) Pearson, E. W.; Gordon, R. G. Local asymptotic gradient corrections to the energy functional of an electron gas. *J. Chem. Phys.* **1985**, *82*, 881−889.
(68) Allan, N. L.; West, C. G.; Cooper, D. L.; Grout, P. J.; March, N. H. The gradient expansions of the kinetic energy and the mean momentum for light diatomic molecules. *J. Chem. Phys.* **1985**, *83*, 4562−4564.
(69) Huang, P.; Carter, E. A. Self-consistent embedding theory for locally correlated configuration interaction wave functions in condensed matter. *J. Chem. Phys.* **2006**, *125*, 084102.
(70) Wang, Y.; Carter, E. A. In *Progress in Theoretical Chemistry and Physics*; Schwartz, S., Ed.; Kluwer: Dordrecht, The Netherlands, 2000; p 117.
(71) Watson, S. C.; Carter, E. A. Linear-scaling parallel algorithms for the first principles treatment of metals. *Comput. Phys. Commun.* **2000**, *128*, 67−92.
(72) Govind, N.; Wang, J.; Guo, H. Total-energy calculations using a gradient-expanded kinetic-energy functional. *Phys. Rev. B* **1994**, *50*, 11175−11178.
(73) Zhou, B.; Ligneres, V. L.; Carter, E. A. Improving the orbital-free density functional theory description of covalent materials. *J. Chem. Phys.* **2005**, *122*, 044103.
(74) Smargiassi, E.; Madden, P. A. Orbital-free kinetic-energy functionals for first-principles molecular dynamics. *Phys. Rev. B* **1994**, *49*, 5220−5226.
(75) Pearson, M.; Smargiassi, E.; Madden, P. A. Ab initio molecular dynamics with an orbital-free density functional. *J. Phys.: Condens. Matter* **1993**, *5*, 3221.
(76) Foley, M.; Madden, P. A. Further orbital-free kinetic-energy functionals for ab initio molecular dynamics. *Phys. Rev. B* **1996**, *53*, 10589−10598.
(77) Xia, J.; Carter, E. A. Density-decomposed orbital-free density functional theory for covalently bonded molecules and materials. *Phys. Rev. B* **2012**, *86*, 235109.
(78) Huang, C.; Carter, E. A. Toward an orbital-free density functional theory of transition metals based on an electron density decomposition. *Phys. Rev. B* **2012**, *85*, 045126.
(79) Snyder, J.; Rupp, M.; Hansen, K.; Müller, K.-R.; Burke, K. Finding density functionals with machine learning. *Phys. Rev. Lett.* **2012**, *108*, 253002.
(80) Gordon, R. G.; Kim, Y. S. Theory for the forces between closed-shell atoms and molecules. *J. Chem. Phys.* **1972**, *56*, 3122−3133.
(81) Senatore, G.; Subbaswamy, K. R. Density dependence of the dielectric constant of rare-gas crystals. *Phys. Rev. B* **1986**, *34*, 5754−5757.
(82) Cortona, P. Self-consistently determined properties of solids without band-structure calculations. *Phys. Rev. B* **1991**, *44*, 8454.

(83) Wesolowski, T. A.; Warshel, A. Frozen density functional approach for ab initio calculations of solvated molecules. *J. Phys. Chem.* **1993**, *97*, 8050.
(84) Wesolowski, T. A. In *Chemistry: Reviews of Current Trends*; Leszczynski, J., Ed.; World Scientific: Singapore, 2006; Vol. *10*, p 1.
(85) Wesolowski, T. A.; Chermette, H.; Weber, J. Accuracy of approximate kinetic energy functionals in the model of Kohn−Sham equations with constrained electron density: The FH-NCH complex as a test case. *J. Chem. Phys.* **1996**, *105*, 9182−9190.
(86) Hodak, M.; Lu, W.; Bernholc, J. Hybrid ab initio Kohn−Sham density functional theory/frozen-density orbital-free density functional theory simulation method suitable for biological systems. *J. Chem. Phys.* **2008**, *128*, 014101.
(87) Elliott, P.; Cohen, M. H.; Wasserman, A.; Burke, K. Density functional partition theory with fractional occupations. *J. Chem. Theory Comput.* **2009**, *5*, 827.
(88) Neugebauer, J. Chromophore-specific theoretical spectroscopy: From subsystem density functional theory to mode-specific vibrational spectroscopy. *Phys. Rep.* **2010**, *489*, 1.
(89) Laricchia, S.; Fabiano, E.; Della Sala, F. Frozen density embedding with hybrid functionals. *J. Chem. Phys.* **2010**, *133*, 164111.
(90) Laricchia, S.; Fabiano, E.; Della Sala, F. Frozen density embedding calculations with the orbital-dependent localized Hartree−Fock Kohn−Sham potential. *Chem. Phys. Lett.* **2011**, *518*, 114−118.
(91) Goodpaster, J. D.; Ananth, N.; Manby, F. R.; Miller, T. F., III Exact nonadditive kinetic potentials for embedded density functional theory. *J. Chem. Phys.* **2010**, *133*, 084103.
(92) Wesolowski, T. A.; Warshel, A. Kohn−Sham equations with constrained electron density: An iterative evaluation of the ground-state electron density of interacting molecules. *Chem. Phys. Lett.* **1996**, *248*, 71.
(93) Laricchia, S.; Fabiano, E.; Della Sala, F. On the accuracy of frozen density embedding calculations with hybrid and orbital-dependent functionals for non-bonded interaction energies. *J. Chem. Phys.* **2012**, *137*, 014102.
(94) Laricchia, S.; Fabiano, E.; Della Sala, F. Semilocal and hybrid density embedding calculations of ground-state charge-transfer complexes. *J. Chem. Phys.* **2013**, *138*, 124112.
(95) Ernzerhof, M. The role of the kinetic energy density in approximations to the exchange energy. *J. Mol. Struct.: THEOCHEM* **2000**, *501*−*502*, 59−64.
(96) Perdew, J. P.; Kurth, S.; Zupan, A.; Blaha, P. Accurate density functional with correct formal properties: A step beyond the generalized gradient approximation. *Phys. Rev. Lett.* **1999**, *82*, 2544.
(97) Tao, J.; Perdew, J. P.; Staroverov, V. N.; Scuseria, G. E. Climbing the density functional ladder: Nonempirical meta-generalized gradient approximation designed for molecules and solids. *Phys. Rev. Lett.* **2003**, *91*, 146401.
(98) Yang, W.; Parr, R. G.; Lee, C. Various functionals for the kinetic energy density of an atom or molecule. *Phys. Rev. A* **1986**, *34*, 4586.
(99) Hoffmann-Ostenhof, T.; Hoffmann-Ostenhof, M. Bounds to expectation values and exponentially decreasing upper bounds to the one-electron density of atoms. *J. Phys. B* **1978**, *11*, 17.
(100) Lee, D.; Constantin, L. A.; Perdew, J. P.; Burke, K. Condition on the Kohn−Sham kinetic energy and modern parametrization of the Thomas−Fermi density. *J. Chem. Phys.* **2009**, *130*, 034107.
(101) Fabiano, E.; Constantin, L. A. Relevance of coordinate and particle-number scaling in density-functional theory. *Phys. Rev. A* **2013**, *87*, 012511.
(102) Heilmann, O. J.; Lieb, E. H. Electron density near the nucleus of a large atom. *Phys. Rev. A* **1995**, *52*, 3628.
(103) Elliott, P.; Burke, K. Non-empirical derivation of the parameter in the B88 exchange functional. *Can. J. Chem.* **2009**, *87*, 1485.
(104) Elliott, P.; Lee, D.; Cangi, A.; Burke, K. Semiclassical origins of density functionals. *Phys. Rev. Lett.* **2008**, *100*, 256406.
(105) Chan, G. K.-L.; Handy, N. C. Kinetic-energy systems, density scaling, and homogeneity relations in density-functional theory. *Phys. Rev. A* **1999**, *59*, 2670−2679.
(106) Nagy, A. Density scaling and exchange-correlation energy. *J. Chem. Phys.* **2005**, *123*, 044105.
(107) Cohen, A. J.; Mori-Sánchez, P.; Yang, W. Challenges for density functional theory. *Chem. Rev.* **2012**, *112*, 289−320.
(108) Liu, S.; Parr, R. G. Expansions of density functionals in terms of homogeneous functionals: Justification and nonlocal representation of the kinetic energy, exchange energy,and classical Coulomb repulsion energy for atoms. *Phys. Rev. A* **1997**, *55*, 1792−1798.
(109) Parr, R. G.; Liu, S. Some functional relations in the density functional theory of finite interacting electronic systems. *Chem. Phys. Lett.* **1997**, *276*, 164−166.
(110) Cohen, A. J.; Mori-Sánchez, P.; Yang, W. Fractional spins and static correlation error in density functional theory. *J. Chem. Phys.* **2008**, *129*, 121104.
(111) Cohen, A. J.; Mori-Sánchez, P.; Yang, W. Insights into current limitations of density functional theory. *Science* **2008**, *321*, 792−794.
(112) Borgoo, A.; Tozer, D. J. Density scaling of noninteracting kinetic energy functionals. *J. Chem. Theory Comput.* **2013**, *9*, 2250−2255.
(113) Kohn, W.; Sham, L. Self-consistent equations including exchange and correlation effects. *Phys. Rev.* **1965**, *140*, A1133.
(114) Clementi, E.; Roetti, C. Roothaan−Hartree−Fock atomic wavefunctions: Basis functions and their coefficients for ground and certain excited states of neutral and ionized atoms, $Z \leq 54$. *Atomic Data Nucl. Data Tables* **1974**, *14*, 177.
(115) Iyengar, S. S.; Ernzerhof, M.; Maximoff, S. N.; Scuseria, G. E. Challenge of creating accurate and effective kinetic-energy functionals. *Phys. Rev. A* **2001**, *63*, 052508.
(116) Biegler-könig, F. W.; Bader, R. F. W.; Tang, T.-H. Calculation of the average properties of atoms in molecules. II. *J. Comput. Chem.* **1982**, *13*, 317−328.
(117) Becke, A. D. Density-functional exchange-energy approximation with correct asymptotic behavior. *Phys. Rev. A* **1988**, *38*, 3098.
(118) Perdew, J. P.; Wang, Y. Accurate and simple analytic representation of the electron-gas correlation energy. *Phys. Rev. B* **1992**, *45*, 13244−13249.
(119) TURBOMOLE V6.2, 2009, a development of University of Karlsruhe and Forschungszentrum Karlsruhe GmbH, 1989−2007, TURBOMOLE GmbH, since 2007; available from http://www.turbomole.com.
(120) Perdew, J. P.; Burke, K.; Ernzerhof, M. Generalized gradient approximation made simple. *Phys. Rev. Lett.* **1996**, *77*, 3865.
(121) Weigend, F.; Ahlrichs, R. Balanced basis sets of split valence, triple zeta valence and quadruple zeta valence quality for H to Rn: Design and assessment of accuracy. *Phys. Chem. Chem. Phys.* **2005**, *7*, 3297.
(122) Rappoport, D.; Furche, F. Property-optimized Gaussian basis sets for molecular response calculations. *J. Chem. Phys.* **2010**, *133*, 134105.
(123) Zhao, Y.; Truhlar, D. G. Design of density functionals that are broadly accurate for thermochemistry, thermochemical kinetics, and nonbonded interactions. *J. Phys. Chem. A* **2005**, *109*, 5656−5667.
(124) Zhao, Y.; Truhlar, D. G. Benchmark databases for nonbonded interactions and their use to test density functional theory. *J. Chem. Theory Comput.* **2005**, *1*, 415−432.
(125) Constantin, L. A.; Fabiano, E.; Della Sala, F. Improving atomization energies of molecules and solids with a spin-dependent gradient correction from one-electron density analysis. *Phys. Rev. B* **2011**, *84*, 233103.
(126) Constantin, L. A.; Fabiano, E.; Della Sala, F. Spin-dependent gradient correction for more accurate atomization energies of molecules. *J. Chem. Phys.* **2012**, *137*, 194105.
(127) Taut, M. Two electrons in an external oscillator potential: Particular analytic solutions of a Coulomb correlation problem. *Phys. Rev. A* **1993**, *48*, 3561.
(128) Constantin, L. A.; Chiodo, L.; Fabiano, E.; Bodrenko, I.; Della Sala, F. Correlation energy functional from jellium surface analysis. *Phys. Rev. B* **2011**, *84*, 045126.

(129) Beyhan, S. M.; Götz, A. W.; Jacob, C. R.; Visscher, L. The weak covalent bond in NgAuF (Ng = Ar, Kr, Xe): A challenge for subsystem density functional theory. *J. Chem. Phys.* **2010**, *132*, 044114.
(130) Jacob, C. R.; Visscher, L. A subsystem density-functional theory approach for the quantum chemical treatment of proteins. *J. Chem. Phys.* **2008**, *128*, 155102.
(131) Kiewisch, K.; Eickerling, G.; Reiher, M.; Neugebauer, J. Topological analysis of electron densities from Kohn−Sham and subsystem density functional theory. *J. Chem. Phys.* **2008**, *128*, 044114.
(132) Govind, N.; Sushko, P.; Hess, W.; Valiev, M.; Kowalski, K. Excitons in potassium bromide: A study using embedded time-dependent density functional theory and equation-of-motion coupled cluster methods. *Chem. Phys. Lett.* **2009**, *470*, 353−357.
(133) Fux, S.; Jacob, C. R.; Neugebauer, J.; Visscher, L.; Reiher, M. Accurate frozen-density embedding potentials as a first step towards a subsystem description of covalent bonds. *J. Chem. Phys.* **2010**, *132*, 164101.
(134) Yan, Z.; Perdew, J. P.; Korhonen, T.; Ziesche, P. Numerical test of the sixth-order gradient expansion for the kinetic energy: Application to the monovacancy in jellium. *Phys. Rev. A* **1997**, *55*, 4601.